Electronic Supplementary Material (ESI) for Journal of Materials Chemistry A.
This journal is © The Royal Society of Chemistry 2019

Supporting Information

Hole Transporting Materials for Perovskite Solar Cells and A Simple Approach for Determining the Performance Limiting Factors

Abasi Abudulimu,*[a] Rafael Sandoval-Torrientes,[a] Iwan Zimmermann,[b] José Santos,*[a,c]
Mohammad K. Nazeeruddin,*[b] Nazario Martín,*[a,c]

[a] *IMDEA Nanociencia, Madrid, 28049, Spain*
[b] *EPFL VALAIS, Sion, 1951, Switzerland*
[c] *Facultad de Ciencias Químicas, Universidad Complutense de Madrid, Madrid, 28040, Spain*

Table of contents

1. Experimental section

General Methods. Chemicals and reagents were purchased from commercial suppliers and used as received. All solvents were dried according to standard procedures. Air-sensitive reactions were carried out under nitrogen atmosphere. The device preparation was done in a glovebox under nitrogen atmosphere. Flash chromatography was performed using silica gel (Fluorochem, Silicagel 60A, 40-63 micron). Analytical thin layer chromatography (TLC) was performed using aluminum-coated Merck Kieselgel 60 F254 plates. NMR spectra were recorded on a Bruker Advance 300 (^{1}H: 400 MHz; ^{13}C: 101 MHz) spectrometer at 298 K using partially deuterated solvents as internal standards. Coupling constants (*J*) are denoted in Hz and chemical shifts (δ) in ppm. Multiplicities are denoted as follows: s = singlet, d = doublet, t = triplet, m = multiplet. UV-vis spectra were recorded in a Varian Cary 50 spectrophotometer. FT-IR spectra were recorded on a Bruker Tensor 27 (ATR device) spectrometer. Mass spectra Matrix assisted Laser desorption ionization (coupled to a Time-of-Flight analyzer) experiments (MALDI-TOF) were recorded on a MAT 95 thermo spectrometer and a Bruker REFLEX spectrometer respectively. Differential scanning calorimetry (DSC) was run on a Discovery DSC from TA instruments. Three cycles were recorded under nitrogen, heating (until 400 °C) and cooling (50 °C) at 20 °C/min of scanning rate. Cyclic voltammetry (CV) experiments were performed in deaerated 0.1 M Bu_4NPF_6 DCM solutions at a scan rate of 100 mV s^{-1}. Glassy carbon was used as a working electrode and platinum wires as counter and reference electrodes. Before each measurement, solutions were deoxygenated with N_2. Ferrocene was added as an internal standard; its oxidation potential in DCM was set at 0.7 V *vs.* NHE, and materials oxidation potentials were recalculated referenced to NHE.

2. Synthetic details and characterization

4,4'-(3,6-Dibromo-9H-fluorene-9,9-diyl)bis(N,N-bis(4-methoxyphenyl)aniline) (3).

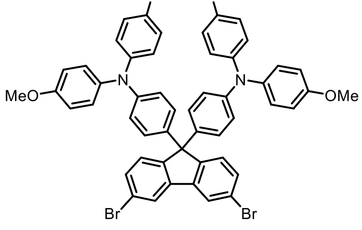

Into a 100 mL 2-neck round bottom flask fitted with a condenser, 3,6-dibromo-9*H*-fluoren-9-one 42 (750 mg, 2.24 mmol), 62 (1.71 g, 5.59 mmol) were dissolved in dry toluene (20 mL), under nitrogen atmosphere. The resulting mixture was heated up to 110 °C, then Eaton's reagent (0.67 mL, 8.87mmol) was added dropwise and the reaction stirred for 18 h. After cooling to room temperature, the mixture was quenched with saturated ammonium chloride solution (20 mL) and extracted with diethyl ether (3 × 15 mL). Combined organic extracts were dried over anhydrous Na_2SO_4, filtered and solvent removed under reduced pressure. Reaction crude was purified by flash chromatography (silica gel, hexane/dichloromethane 1:7) yielding a white solid (1.25 g, 60%). ^{1}H NMR (400 MHz, $CDCl_3$) δ: 7.82 (d, *J* = 1.7 Hz, 2H), 7.40 (dd, *J* = 8.2, 1.8 Hz, 2H), 7.27 (d, *J* = 8.2 Hz, 2H), 7.02 (d, *J* = 7.7 Hz, 8H), 6.93 (d, *J* = 8.5 Hz, 4H), 6.80 (d, *J* = 8.9 Hz, 8H), 6.75 (d, *J* = 8.1 Hz, 4H), 3.78 (s, 12H) ppm. ^{13}C NMR (101 MHz, $CDCl_3$) δ: 156.0, 151.3, 147.7, 140.9, 136.1, 131.2, 128.5, 127.9, 126.8, 123.6, 121.5, 119.9, 114.8, 64.1, 55.6 ppm. HRMS (MALDI-TOF) *m/z*: calculated for $C_{53}H_{42}Br_2N_2O_4$: 930.1455, found: 928.1487. FTIR (neat): 3734, 3618, 3035, 2937, 2831, 1740, 1600, 1495, 1461, 1318.61, 1273, 1233, 1169, 1102, 1028, 873, 815, 758, 718, 665, 631, 571 cm^{-1}. M.p.: 279.0−281.0 °C.

HTM1

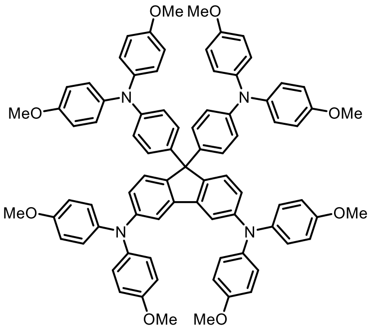

Into a 100 mL 2-neck round bottom flask fitted with a condenser, **3** (1.03 g, 1.10 mmol), **4** (558 mg, 2.43 mmol), $Pd_2(dba)_3$ (25.0 mg, 0.03 mmol), XPhos (52.0 mg, 0.11 mmol) were dissolved in dry toluene (20 mL) under nitrogen atmosphere. The mixture was degassed for 30 min. Then NaO^{t}Bu (317 mg, 3.30 mmol) was added in one portion and the resulting mixture was stirred at 110 °C for 18 h. Upon cooling to room temperature, the mixture was quenched with H_2O (15 mL) and extracted with Et_2O (3 × 10 mL). Combined organic extracts were dried over anhydrous Na_2SO_4, filtered and evaporated under reduced pressure. Reaction crude was purified by flash chromatography (silica gel, dichloromethane/ethyl acetate 20:1) yielding a white powder (742 mg, 55%). ^{1}H NMR (400 MHz, THF-d^8) δ: 7.21 (d, *J* = 2.1 Hz, 2H), 7.17 (d, *J* = 8.3 Hz, 2H), 7.01–6.93 (m, 20H), 6.81–6.74 (m, 18H), 6.70 (d, *J* = 8.7 Hz, 4H), 3.72 (s, 12H), 3.71 (s, 12H) ppm. ^{13}C NMR (101 MHz, THF-d^8) δ: 157.3, 156.9, 149.4, 148.2, 146.5, 142.6, 142.1, 142.0, 139.5, 129.6, 127.6, 127.4, 126.7, 122.8, 120.5, 115.53, 115.5, 114.4, 64.1, 55.7, 55.6 ppm. HRMS (MALDI-TOF) *m/z*: calculated for $C_{81}H_{70}N_4O_8$: 1226.5166, found: 1226.5188. FTIR (neat): 3034, 2998, 2948, 2834, 1743, 1607, 1502, 1453, 1239, 1175, 1106, 1035, 824, 731, 580 cm^{-1}. M.p.: 165.1−167.1 °C.

HTM2

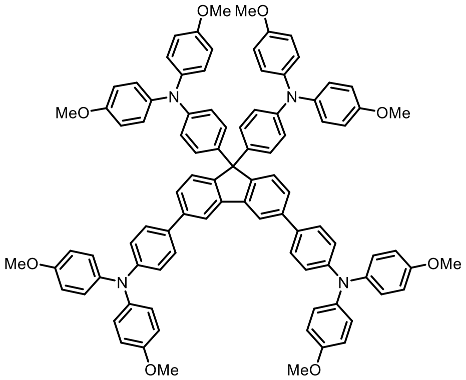

Into a 100 mL 2-neck round bottom flask fitted with a condenser, **3** (173 mg, 0.12 mmol), **5** (176 mg, 0.41 mmol) and $Pd(PPh_3)_4$ (22.0 mg, 0.02 mmol) were dissolved in dry DMF (20 mL) under nitrogen atmosphere, the mixture was then degassed for 30 min. Thereafter, K_3PO_4 (631 mg, 2.97 mmol) was added in one portion and the mixture was stirred at 90 °C for 18 h. Upon cooling to room temperature, the mixture was quenched with H_2O (30 mL). The resulting precipitate was filtered off and washed with water. After vacuum drying the remaining moisture, the crude was purified by flash chromatography (silica gel dichloromethane/ethyl acetate 17:1) yielding a white powder (180 mg, 70%). ^{1}H NMR (400 MHz, THF-d^8) δ: 7.50 (d, *J* = 8.4 Hz, 4H), 7.47–7.39 (m, 4H), 7.10–7.01 (m, 12H), 6.96 (d, *J* = 8.5 Hz, 14H), 6.84 (d, *J* = 8.6 Hz, 8H), 6.77 (d, *J* = 8.7 Hz, 8H), 6.72 (d, *J* = 8.4 Hz, 4H), 3.75 (s, 12H), 3.71 (s, 12H) ppm. ^{13}C NMR (101 MHz, THF-d^8) δ: 157.5, 157.4, 157.2, 151.7, 149.4, 148.4, 142.1, 142.0, 141.8, 141.4, 139.0, 134.4, 129.7, 128.5, 127.6, 127.5, 126.9, 121.6, 120.8, 119.1, 115.6, 115.5, 65.0, 55.8, 55.7 ppm. HRMS (MALDI-TOF) *m/z*: calculated for $C_{93}H_{78}N_4O_8$: 1378.5814, found: 1378.5831. FTIR (neat): 3037, 2925, 2837, 1740, 1606, 1503, 1318, 1274, 1298, 1174, 1106, 1035, 822, 728, 605, 576 cm^{-1}. M.p.: 215.3−217.3 °C.

2,6-Dibromo-4-(dibromomethylene)-4*H*-cyclopenta[2,1-b:3,4-b']dithiophene (7)

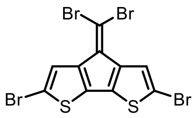

2,6-dibromo-4*H*-cyclopenta[2,1-*b*:3,4-*b*']dithiophen-4-one (200 mg, 0.60 mmol), PPh_3 (640 mg, 2.44 mmol) and CBr_4 (400m g, 1.22 mmol) were dissolved in dry CH_2Cl_2 (15 mL). The reaction mixture was stirred for 30 minutes at room temperature, thereafter, distilled water (15 mL) was added to quench the reaction. The organic layer was separated, washed with water, dried over anhydrous Na_2SO_4, filtered and evaporated under reduced pressure. The reaction crude was purified by flash chromatography (silica gel, hexane/dichloromethane 1:1) yielding a pink solid (160 mg, 55%). ^{1}H NMR (400 MHz, $CDCl_3$) δ: 7.63 (s, 2H) ppm. ^{13}C NMR (101 MHz, $CDCl_3$) δ: 141.2, 136.5, 129.9, 126.7, 111.1, 96.5 ppm. HRMS (MALDI-TOF) *m/z*: calculated for $C_{10}H_2Br_4S_2$: 505.6294, found: 505.6284. FTIR (neat): 3101, 2921, 2850, 1614, 1575, 1459, 1366, 1302, 1270, 1182, 1046, 942, 901, 829, 756, 694, 626 cm^{-1}. M.p.: decomp >300 ºC.

HTM3

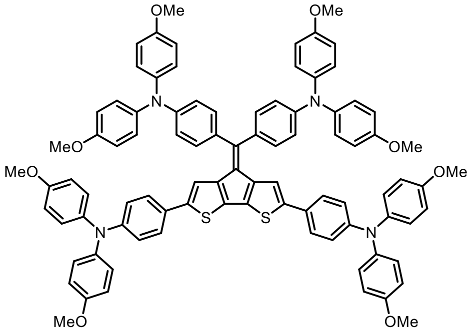

Into a 100 mL 2-neck round bottom flask, **7** (60 mg, 0.14 mmol), **5** (300 mg, 0.69 mmol), Pd(PPh$_3$)$_4$ (30 mg, 0.03 mmol), and Na$_2$CO$_3$ (230 mg 2.24 mmol) were added to a 5:1 THF/H$_2$0 mixture (25 mL) under nitrogen atmosphere. The mixture was degassed for 40 min and then stirred at 90 ^{o}C for 4 h. Upon completion, THF was removed under reduced pressure, and CHCl$_3$ (50 mL) added. The organic layer was washed with H$_2$O (3 × 50 mL), dried over anhydrous Na$_2$SO$_4$ and filtered. After removing the solvent under reduced pressure, the reaction crude was purified by flash chromatography (silica gel, hexane/ethyl acetate 4:1) yielding a dark brown solid (100 mg 50%). ^{1}H NMR (400 MHz, THF-d^8) δ: 7.25 (t, *J* = 8.2 Hz, 8H), 7.08 (dd, *J* = 18.2, 8.7 Hz, 16H), 6.92 (dd, *J* = 8.6, 2.3 Hz, 8H), 6.84 (dd, *J* = 17.4, 8.8 Hz, 16H), 6.58 (s, 2H), 3.76 (s, 12H), 3.71 (s, 12H) ppm.^{13}C NMR (101 MHz, THF-d^8) δ :157.8, 157.5, 151.0, 149.1, 146.6, 143.2, 141.8, 141.5, 133.95, 133.6, 128.8, 127.9, 127.5, 126.5, 121.7, 120.1, 119.1, 115.8, 115.7, 55.8, 55.76 ppm. HRMS (MALDI-TOF) *m/z*: calculated for $C_{90}H_{74}N_4O_8S_2$: 1402.4944, found 1402.4943. FTIR (neat): 2998, 2935, 2830 1740, 1595, 1497, 1317, 1273, 1231, 1167, 1103, 1029, 819, 757, 629, 575 cm^{-1}.

3. NMR, FTIR & MS spectra

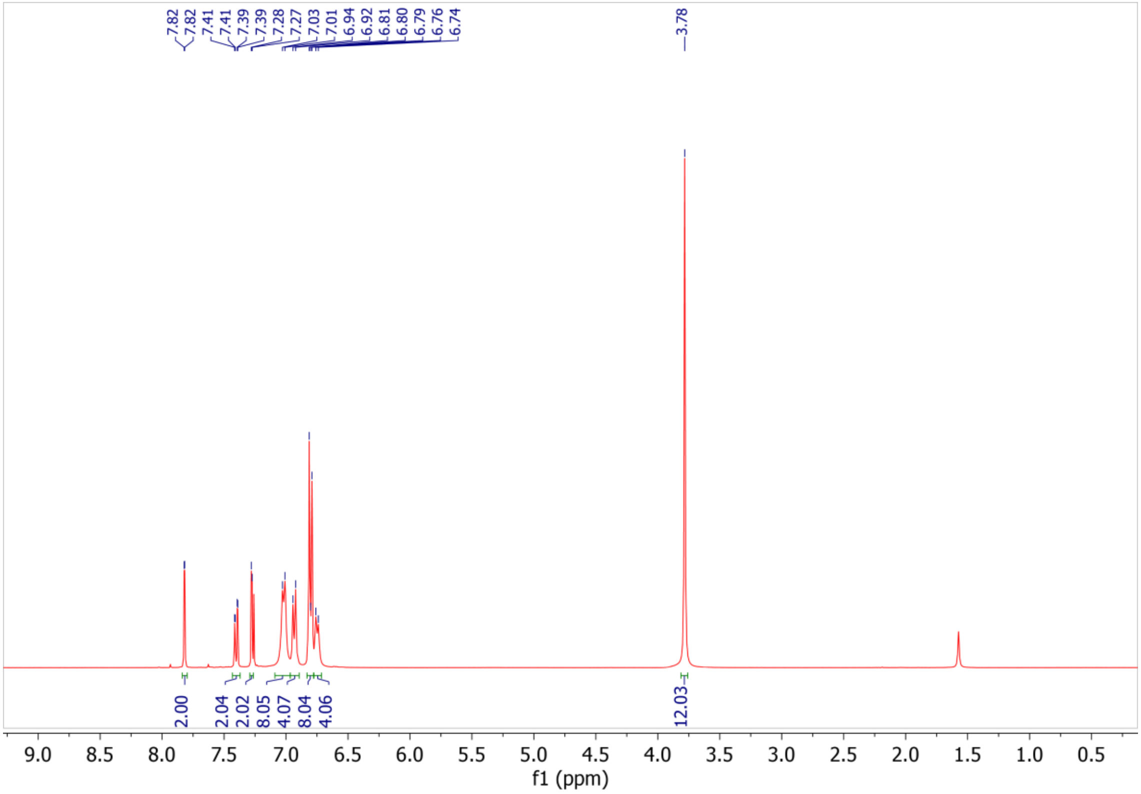

Figure S1. ^{1}H NMR (400 MHz, CDCl$_3$, 298 K) of compound **3**.

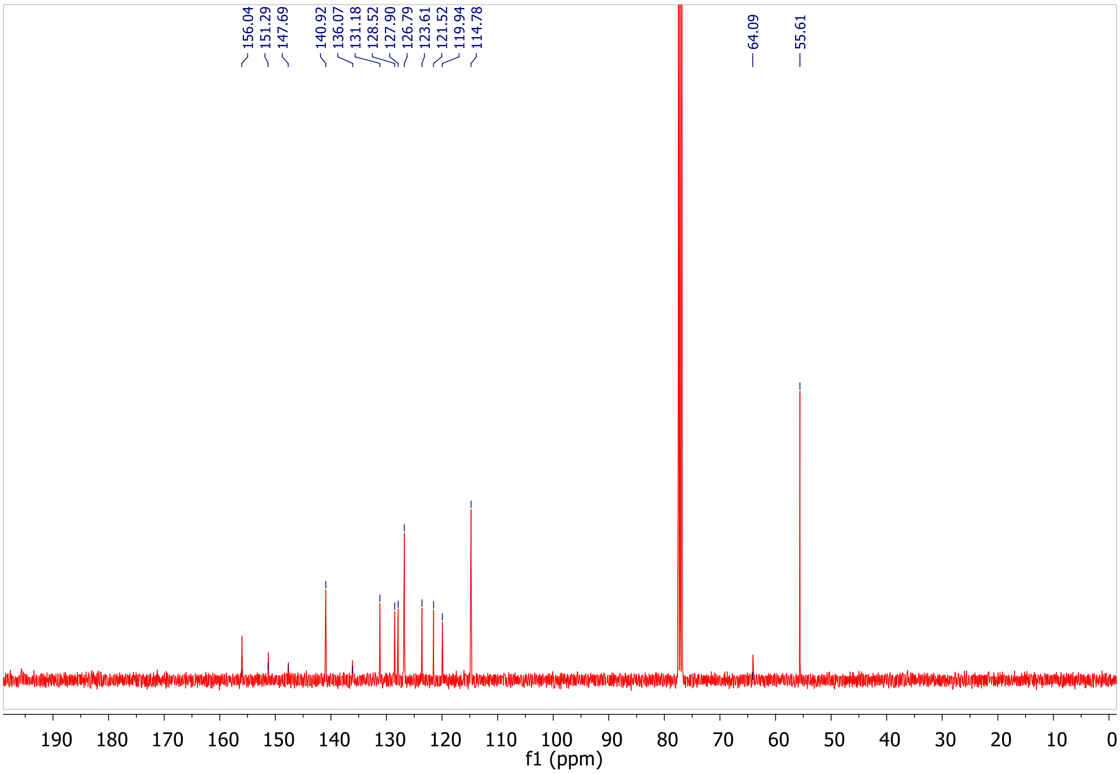

Figure S2. ^{13}C NMR (101 MHz, CDCl$_3$, 298 K) of compound **3**.

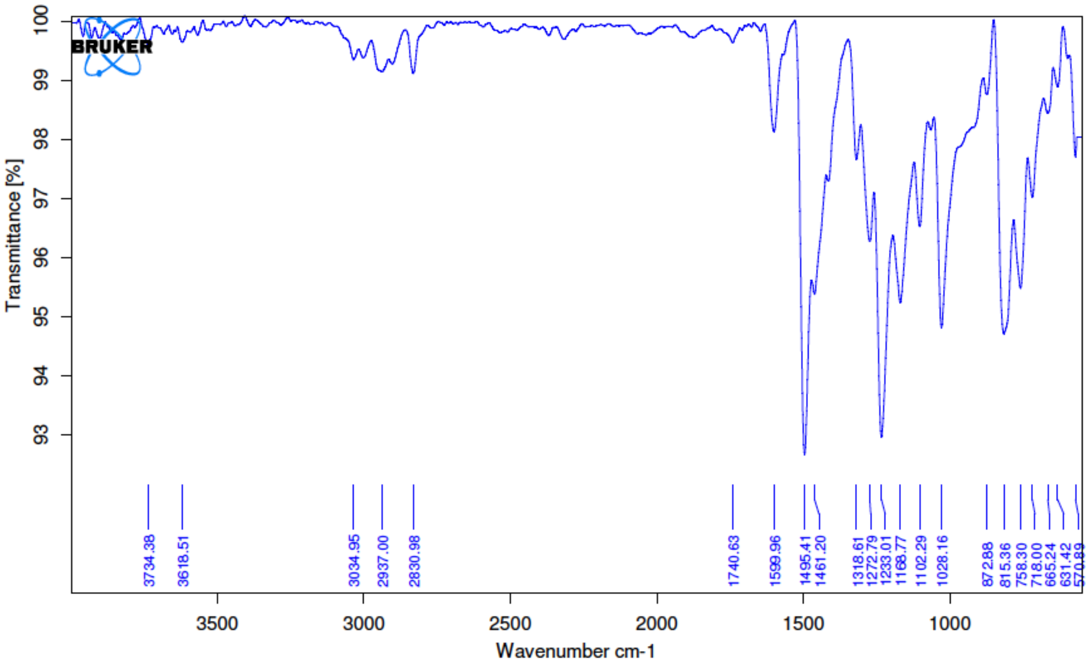

Figure S3. FTIR of compound **3**.

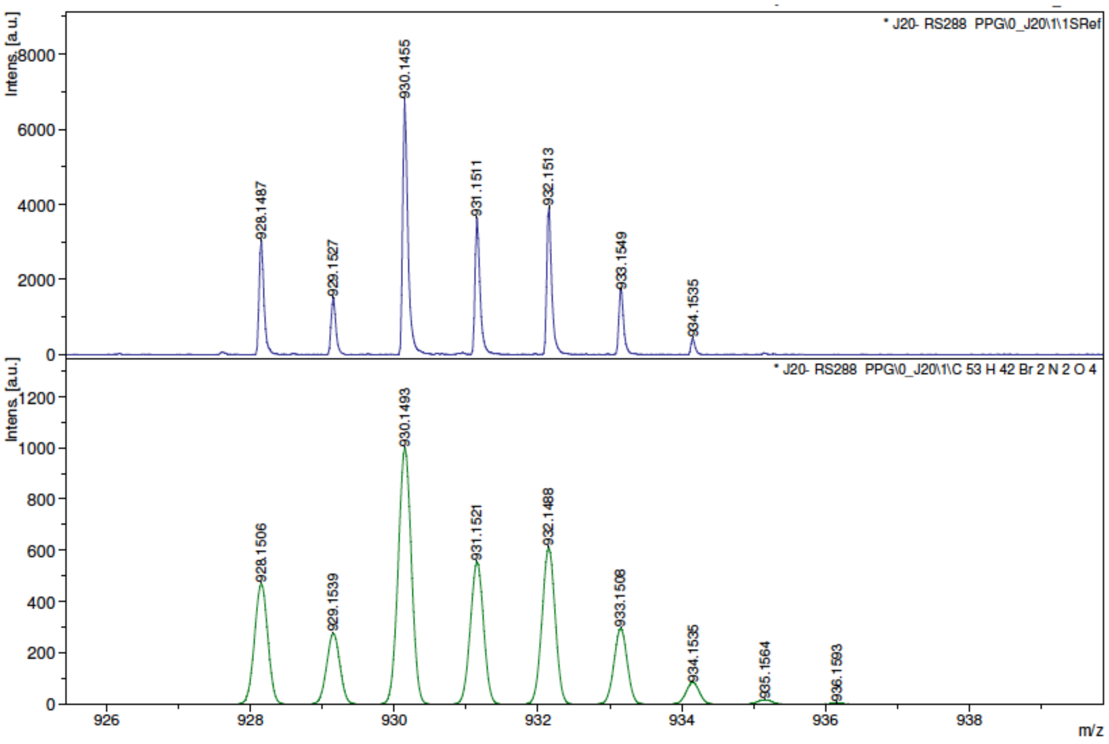

Figure S4. MALDI-TOF mass spectrum of **3**.

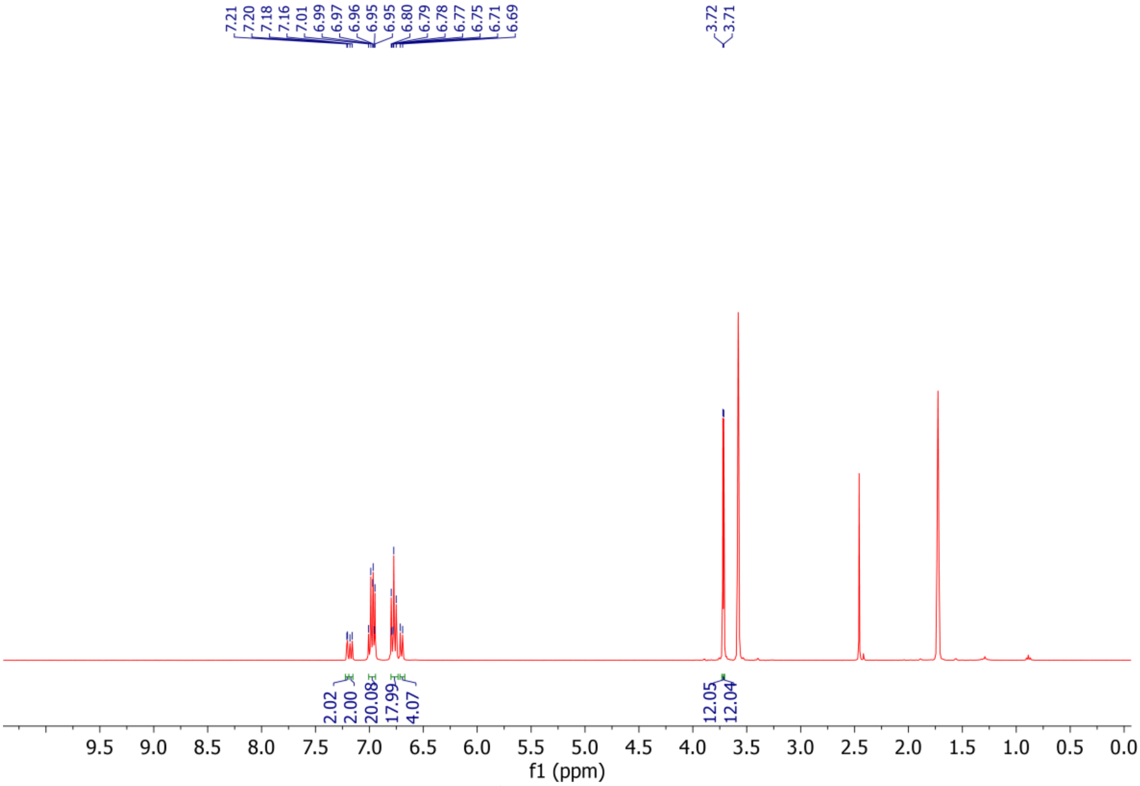

Figure S5. ^{1}H NMR (400 MHz, THF-d^{8}, 298 K) of compound **HTM1**.

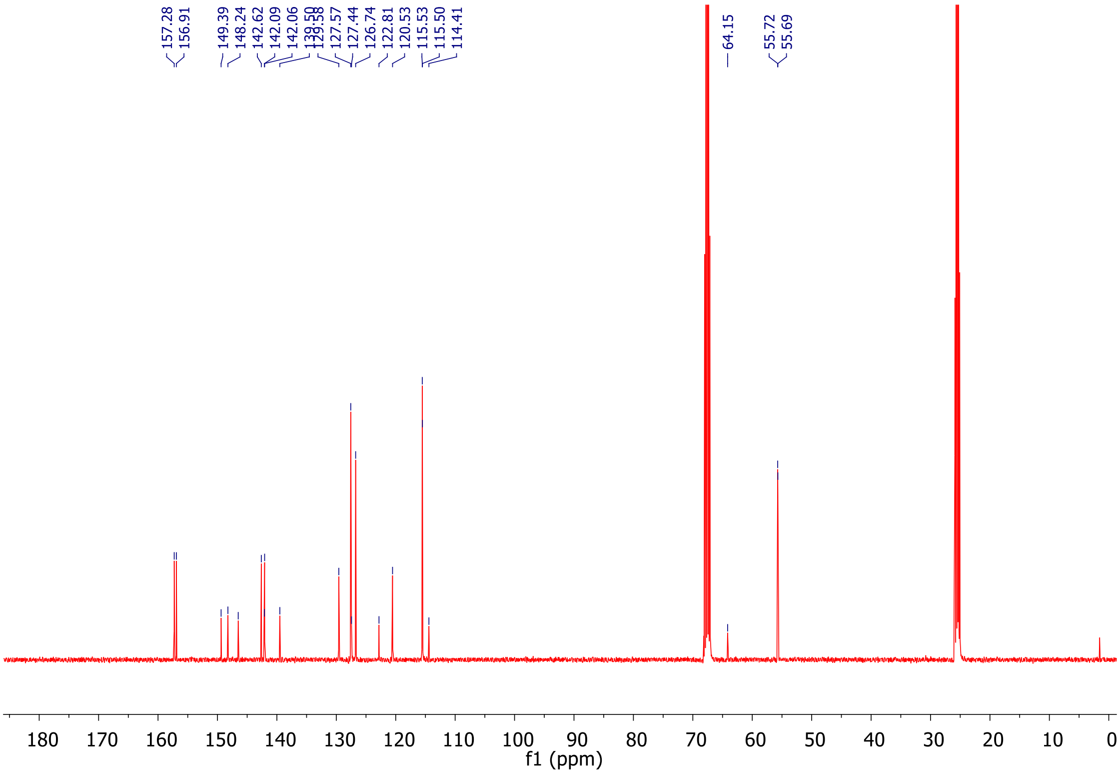

Figure S6. ^{13}C NMR (101 MHz, THF-d^{8}, 298 K) of compound **HTM1**.

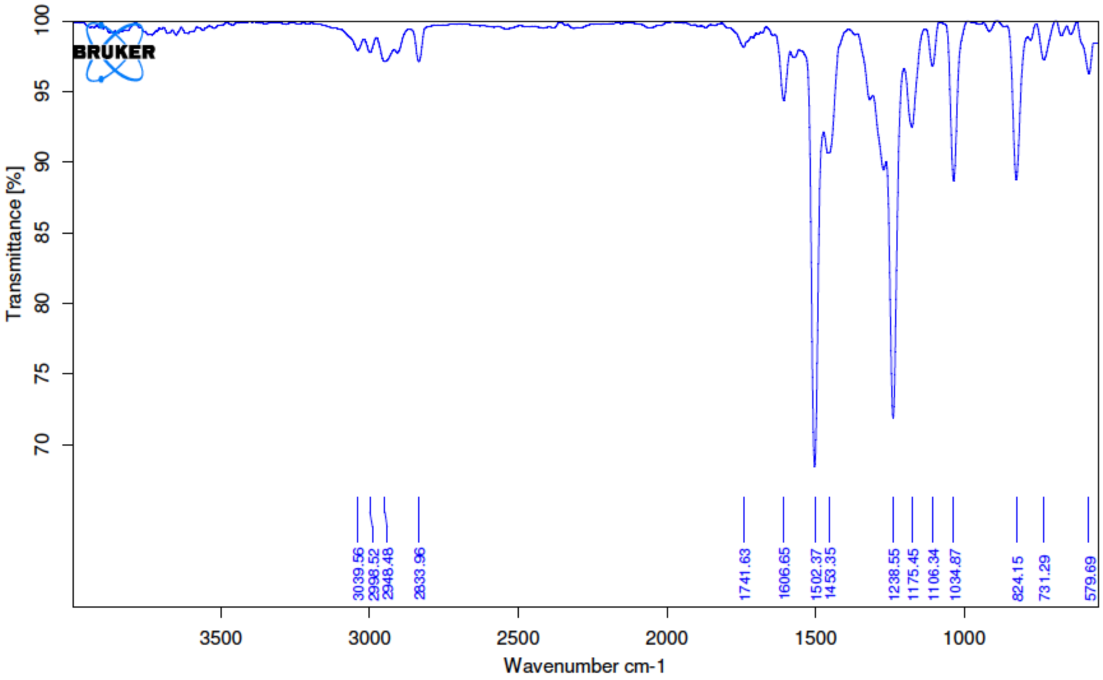

Figure S7. FTIR of compound **HTM1**.

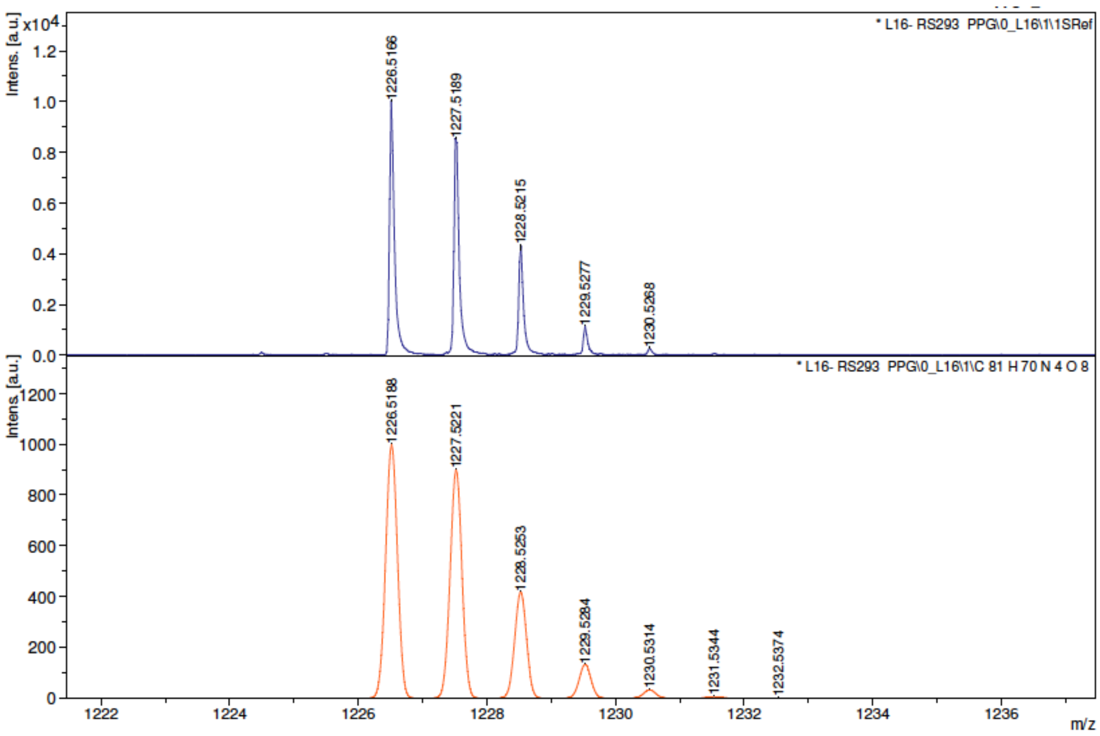

Figure S8. MALDI-TOF mass spectrum of **HTM1**.

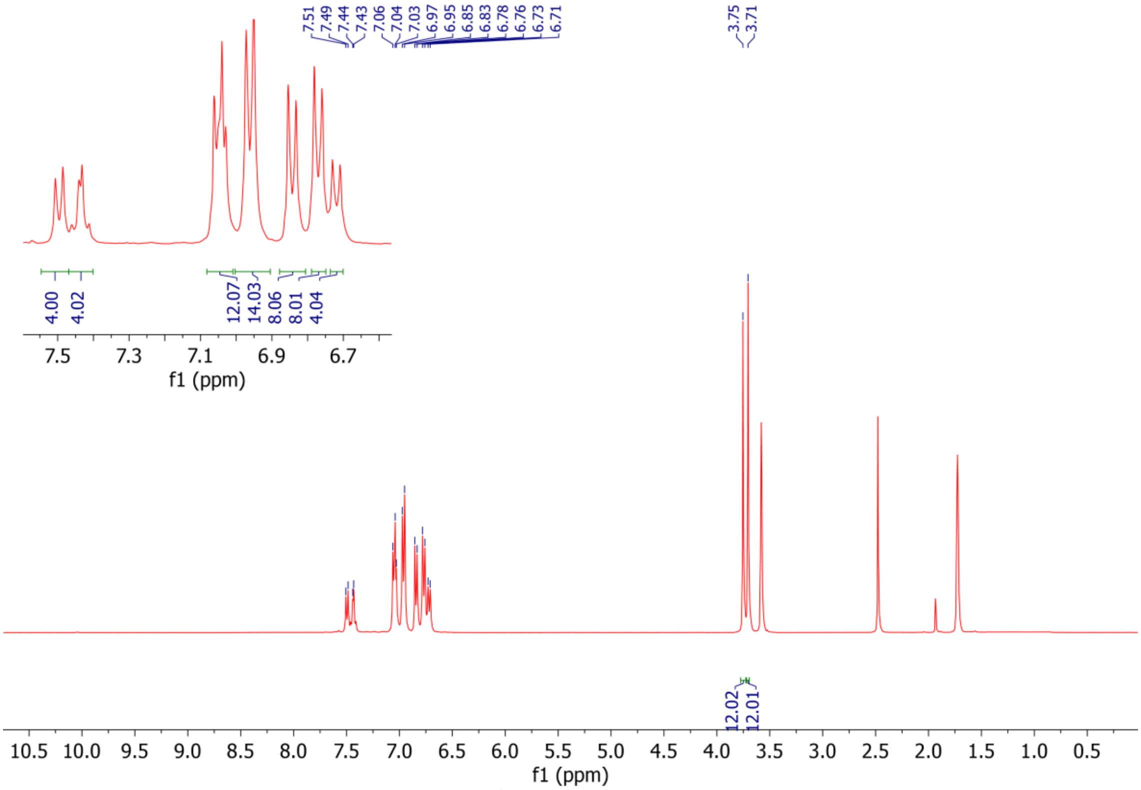

Figure S9. ^{1}H NMR (400 MHz, THF-d^8, 298 K) of compound **HTM2**.

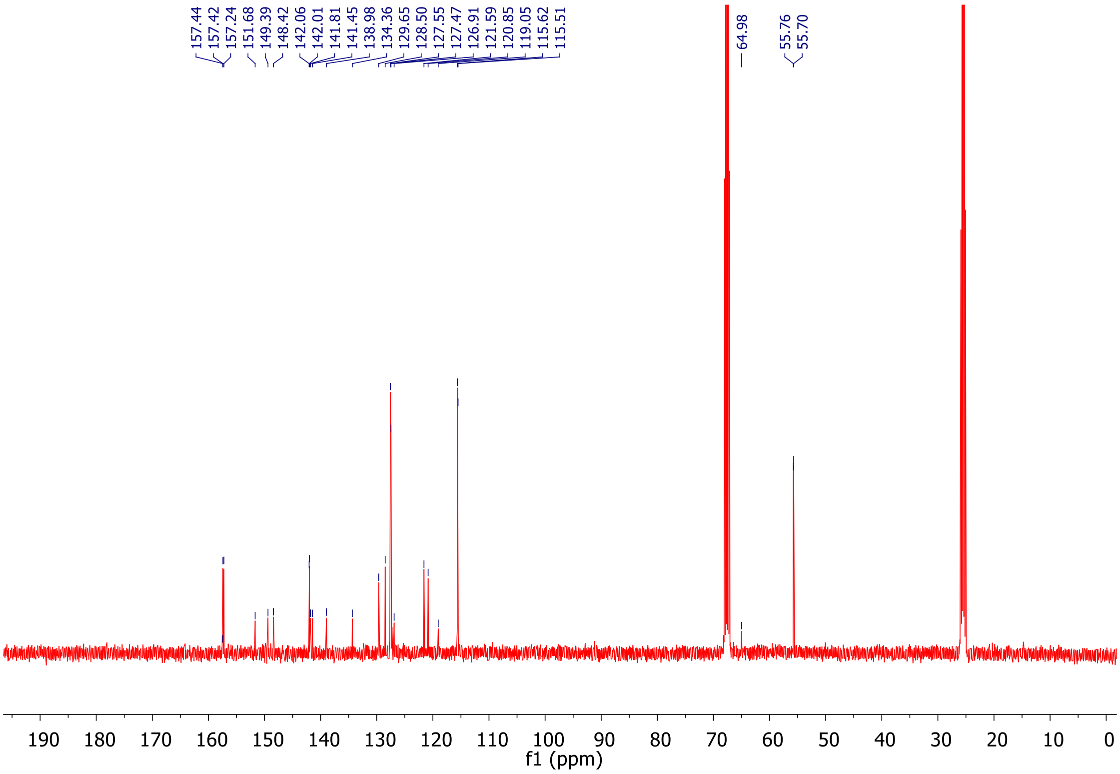

Figure S10. ^{13}C NMR (101 MHz, THF-d^8, 298 K) of compound **HTM2**.

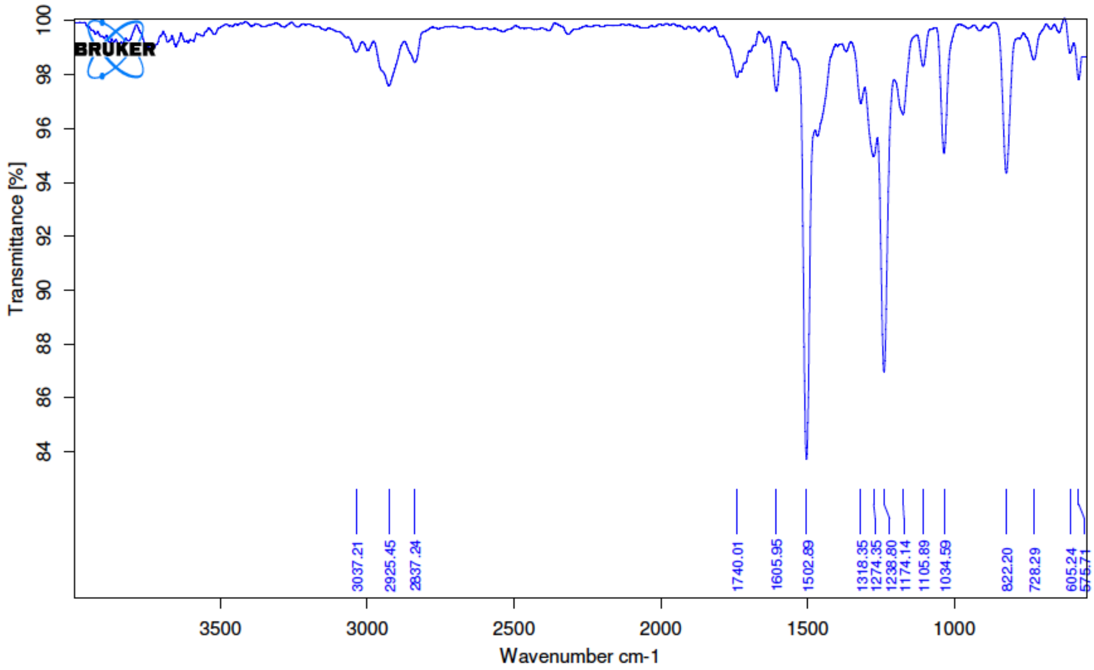

Figure S11. FTIR of compound **HTM2**.

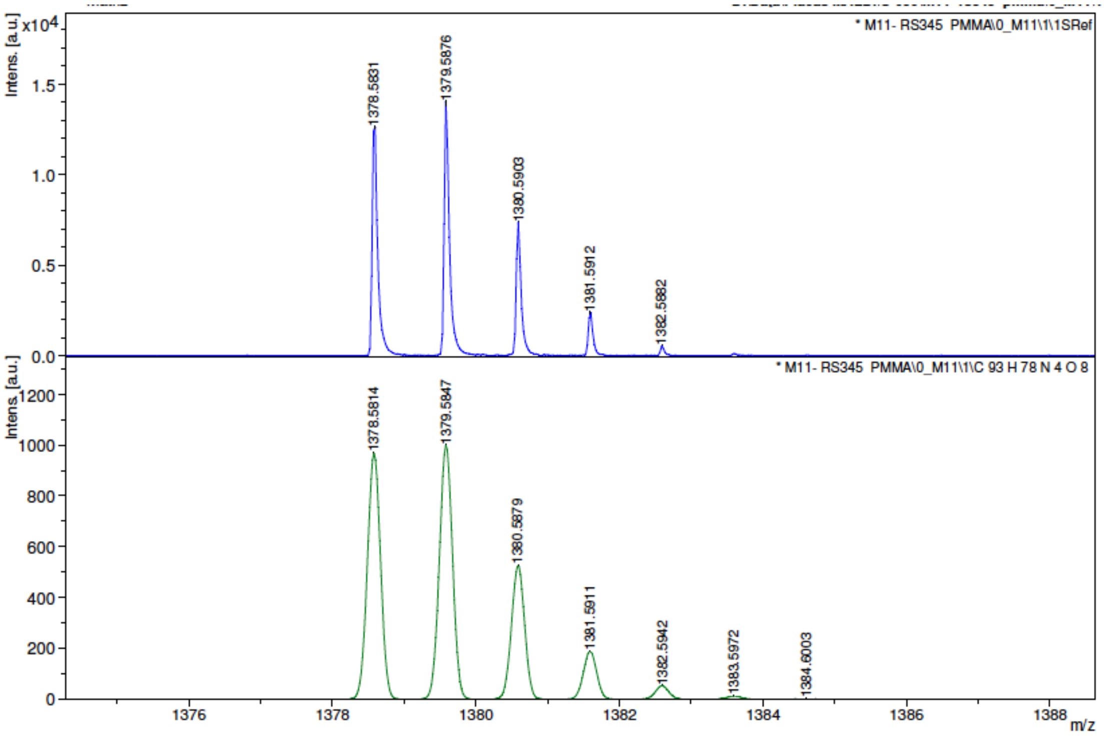

Figure S12. MALDI-TOF mass spectrum of **HTM2**.

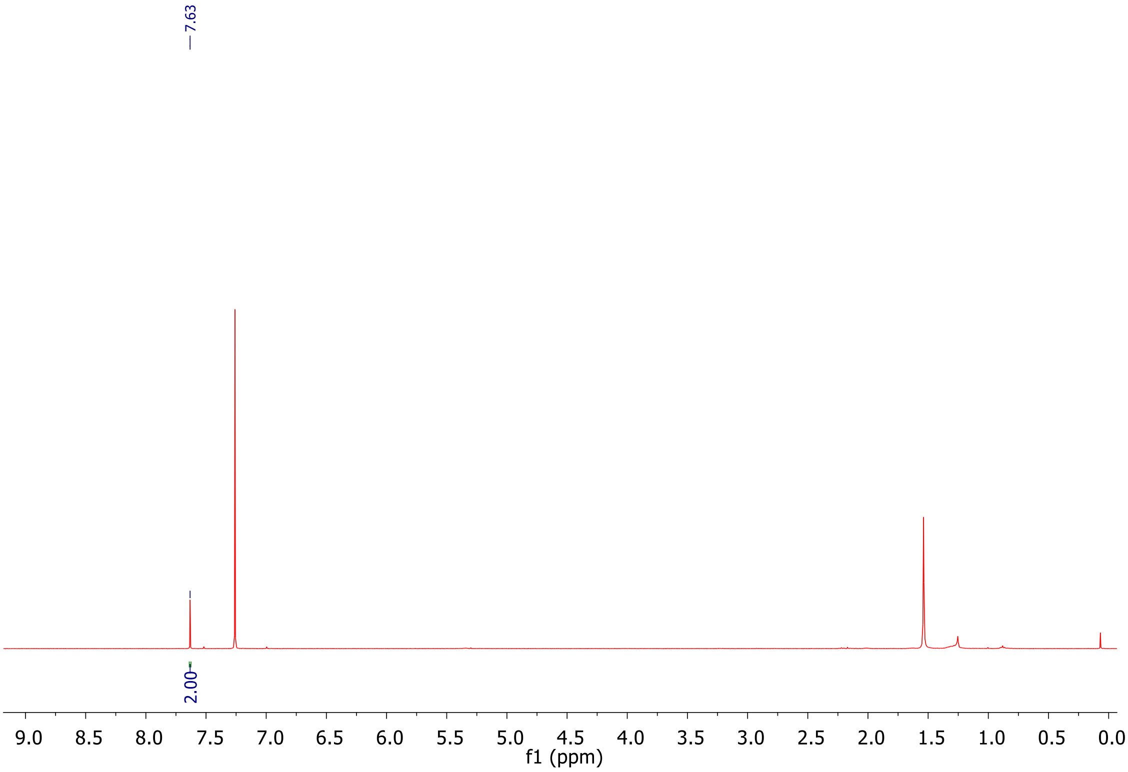

Figure S13. ^{1}H NMR (400 MHz, $CDCl_3$, 298 K) of compound **7**.

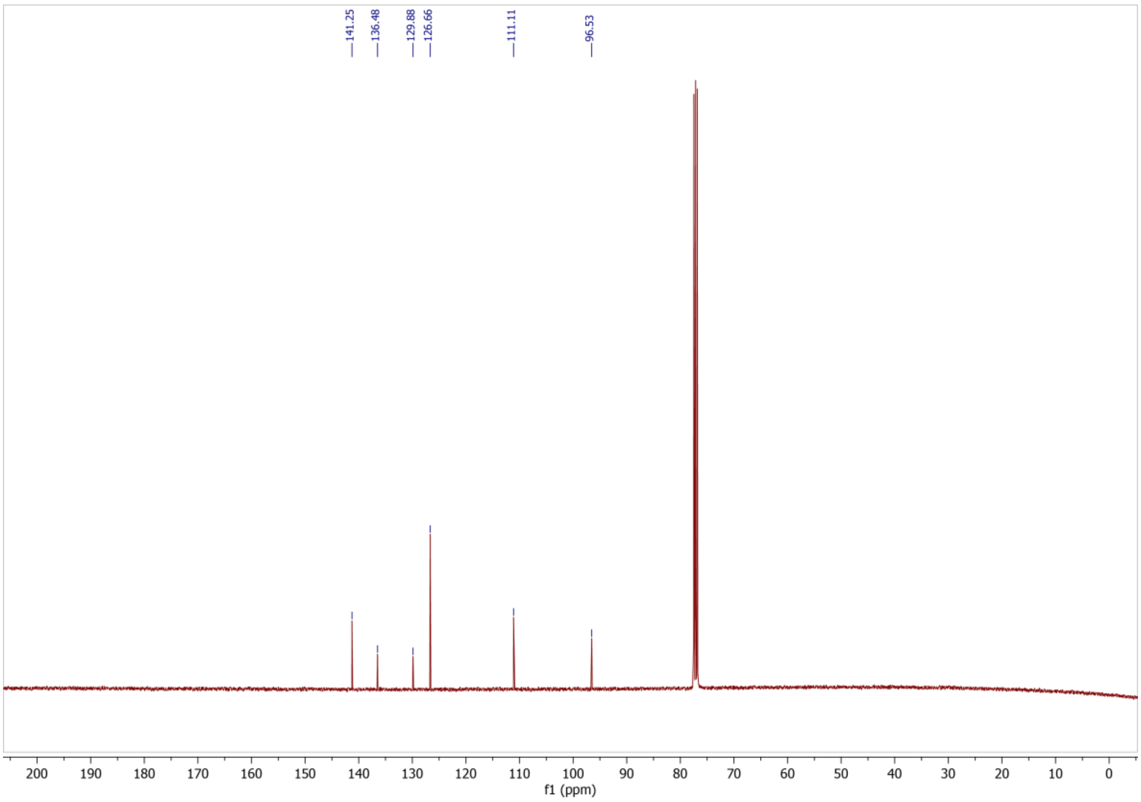

Figure S14. ^{13}C NMR (101 MHz, $CDCl_3$, 298 K) of compound **7**.

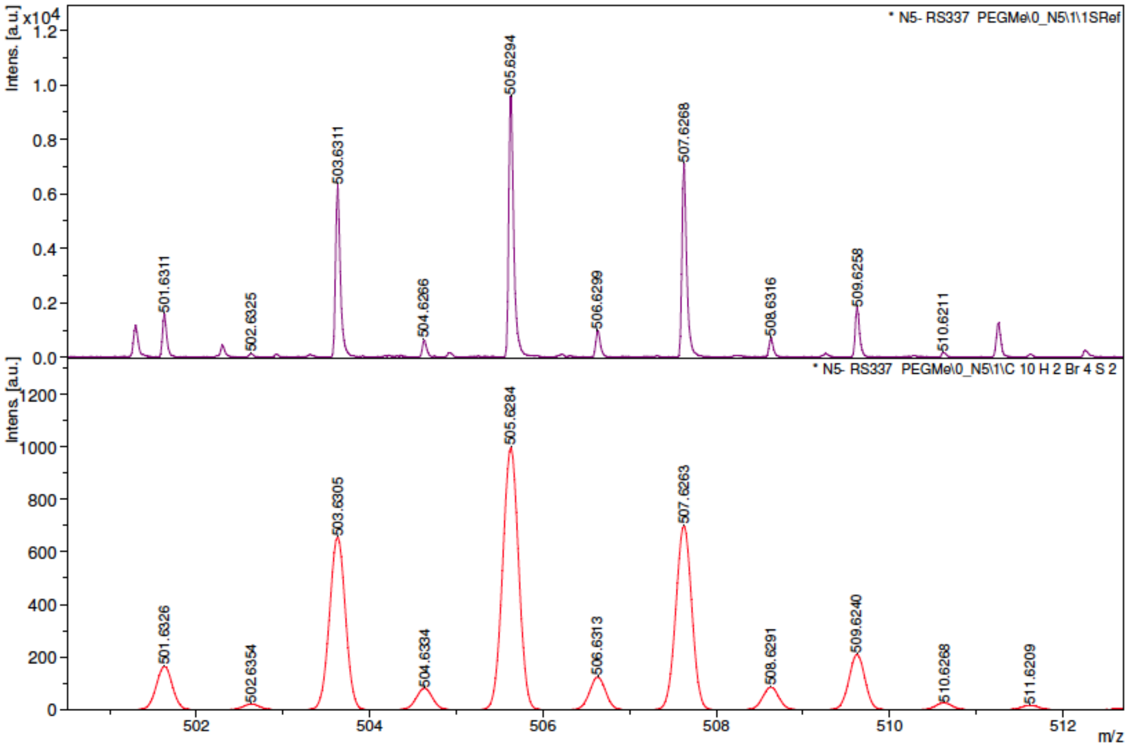

Figure S15. MALDI-TOF mass spectrum of **7**.

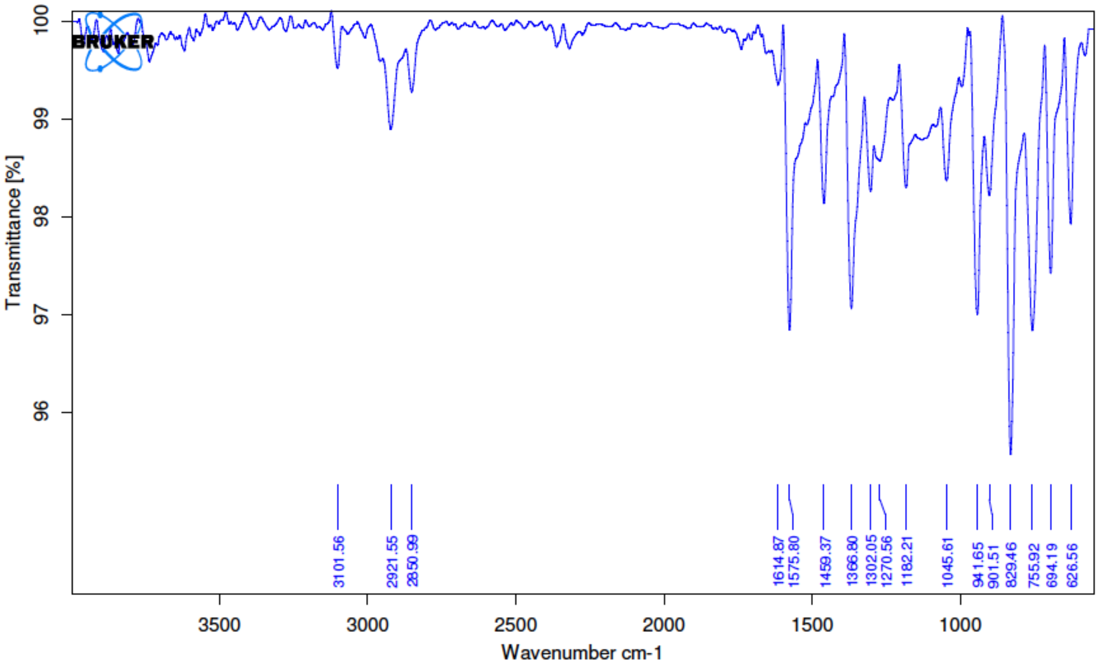

Figure S16. FTIR of compound **7**.

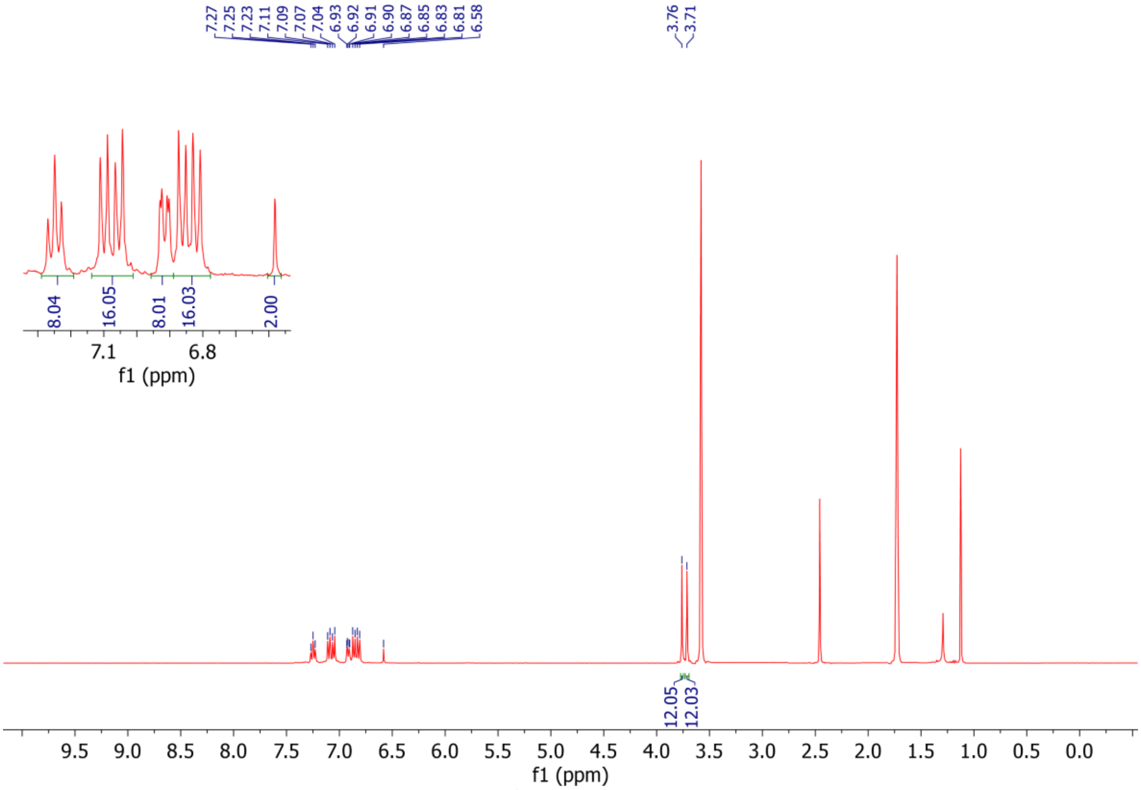

Figure S17. ^{1}H NMR (400 MHz, THF-d^8, 298 K) of compound **HTM3**.

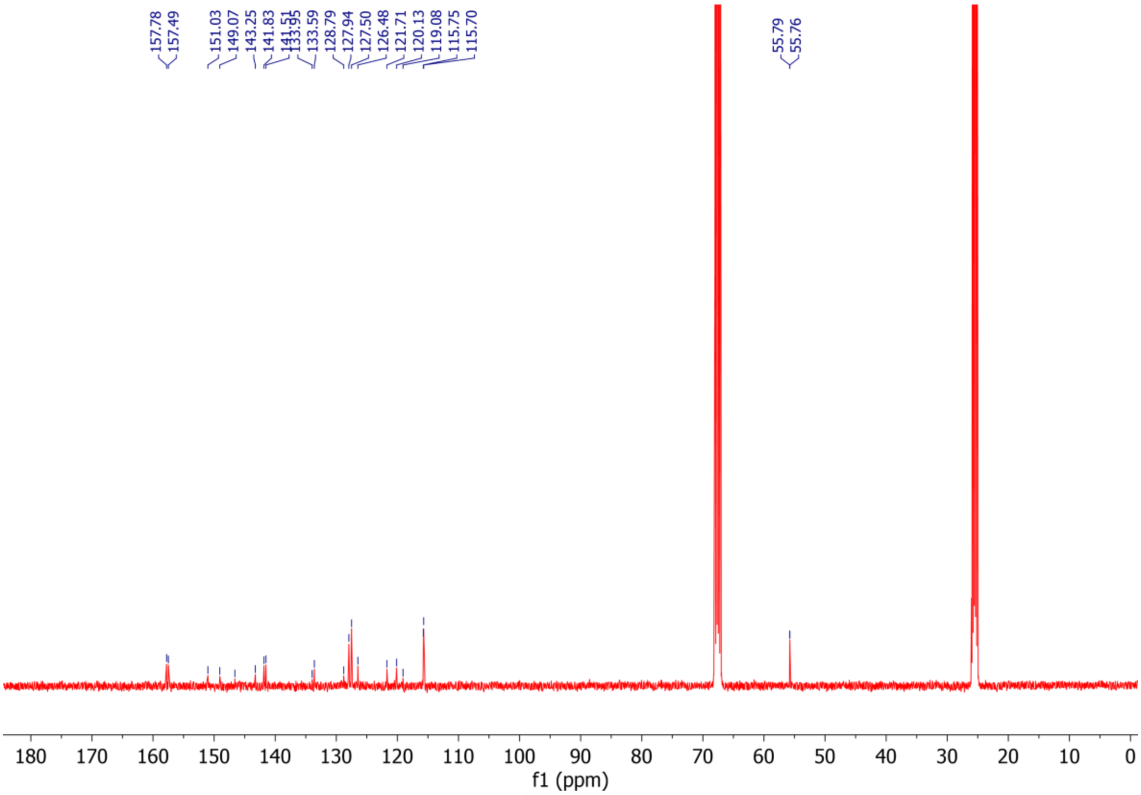

Figure S18. ^{13}C NMR (101 MHz, THF-d^8, 298 K) of compound **HTM3**.

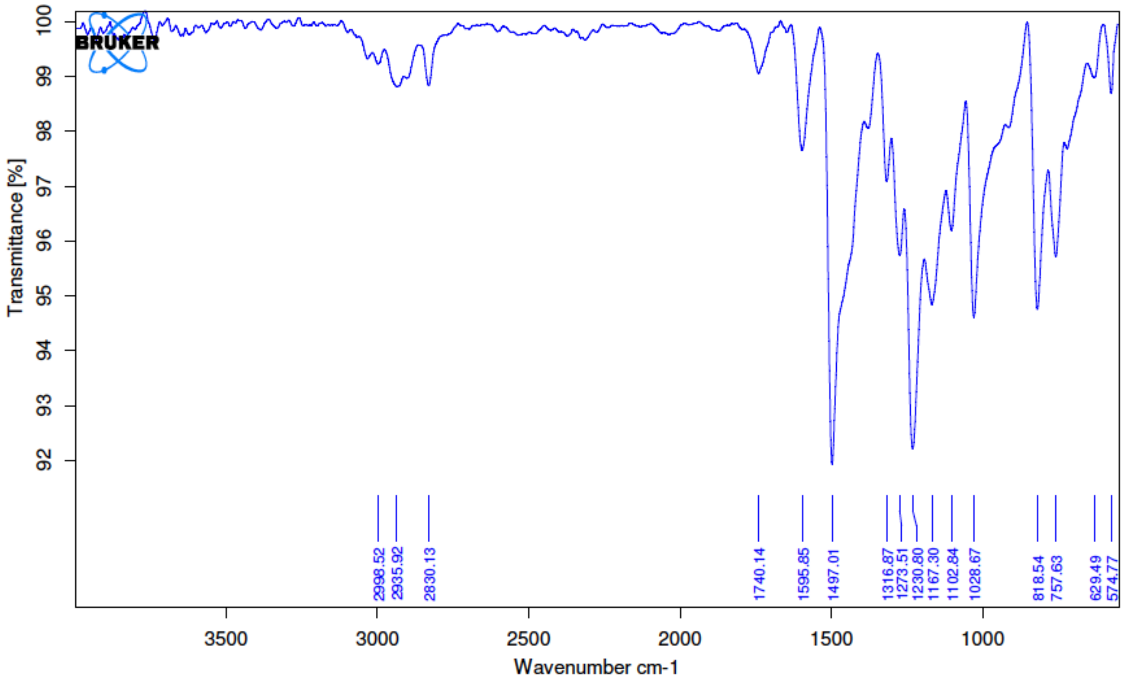

Figure S19. FTIR of compound **HTM3**.

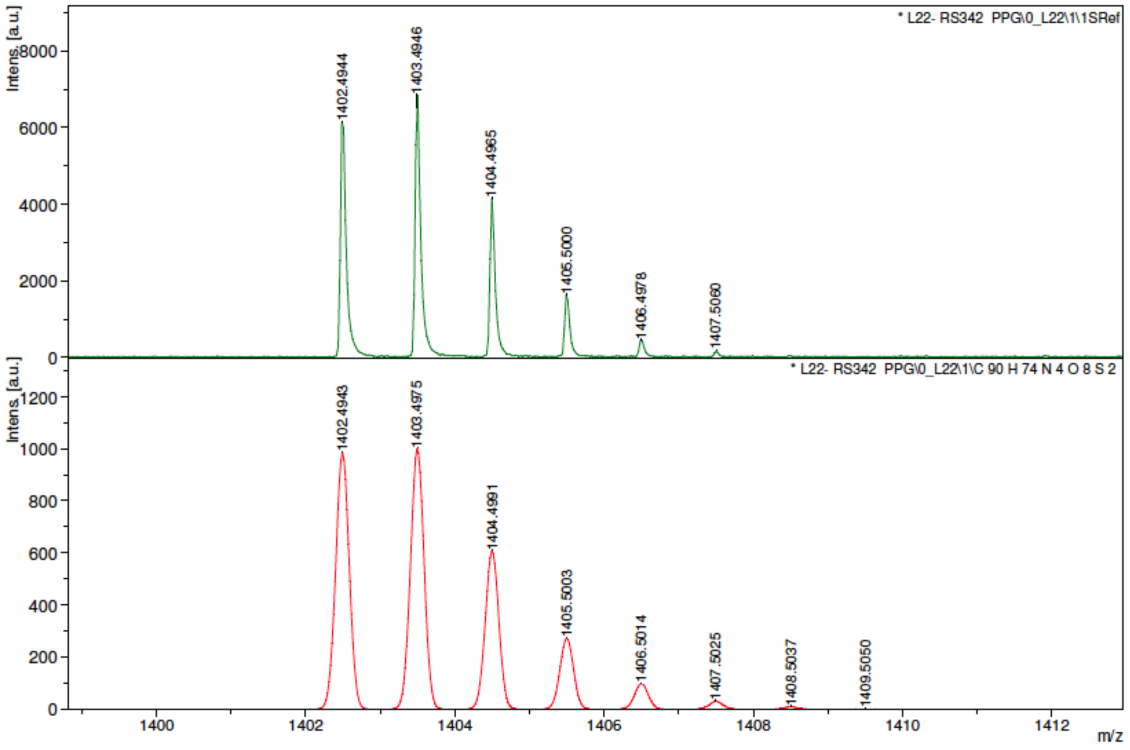

Figure S20. MALDI-TOF mass spectrum of **HTM3**.

4. Optical properties

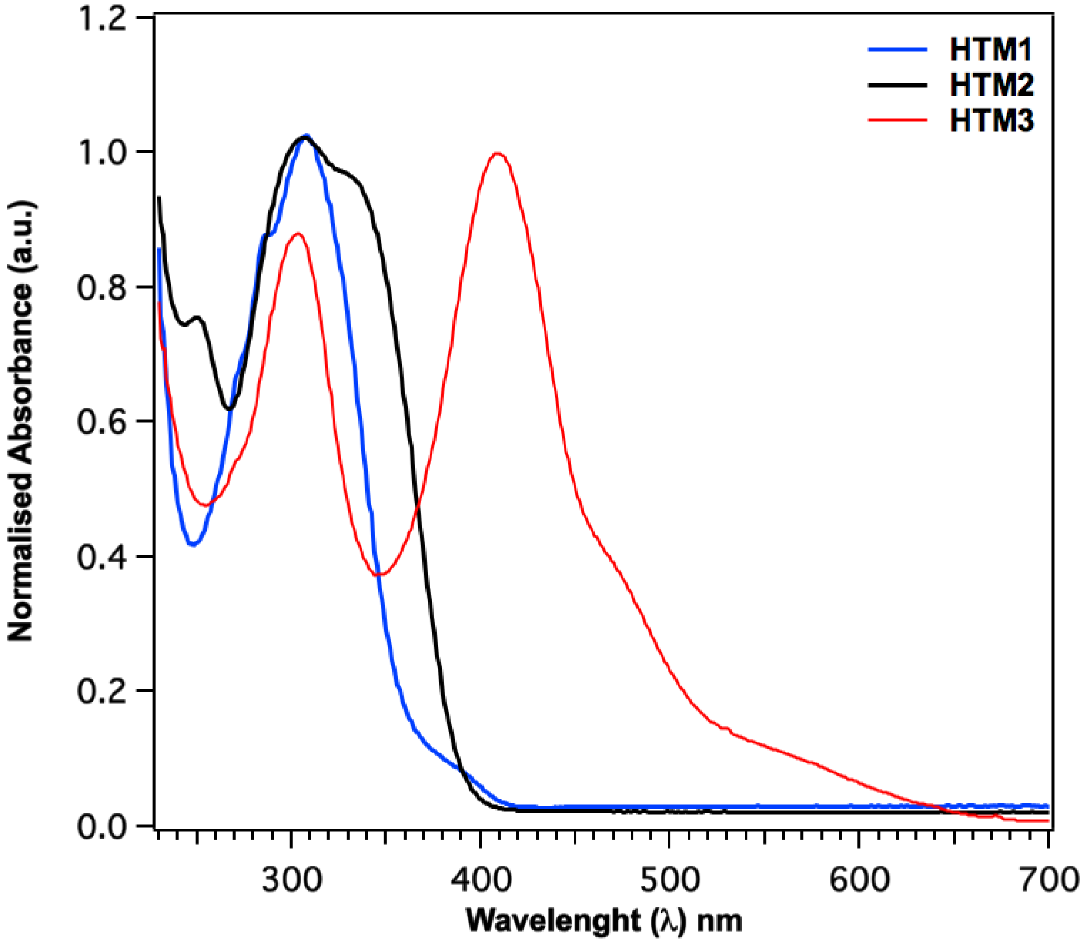

Figure S21. UV-Vis spectra of **HTM1**, **HTM2** and **HTM3** in DCM solution (10^{-5}M).

Table S1. Optical properties of **HTM1**, **HTM2** and **HTM3**.

Compounds	λ_{max} [nm]^a	λ_{onset} [nm]^a	E_{gap}^{opt} [eV]^a	$\varepsilon \times 10^4$ [$M^{-1}cm^{-1}$]^b
HTM1	308	365	3.39	11.1
HTM2	306	390	3.17	7.90
HTM3	404	640	1.93	6.66

[a] Measured in DCM solution, $E_{gap}^{opt} = 1240/\lambda_{onset}$ [eV]; [b] Molar absorption of the lower energy band in DCM solution.

5. Electrochemistry

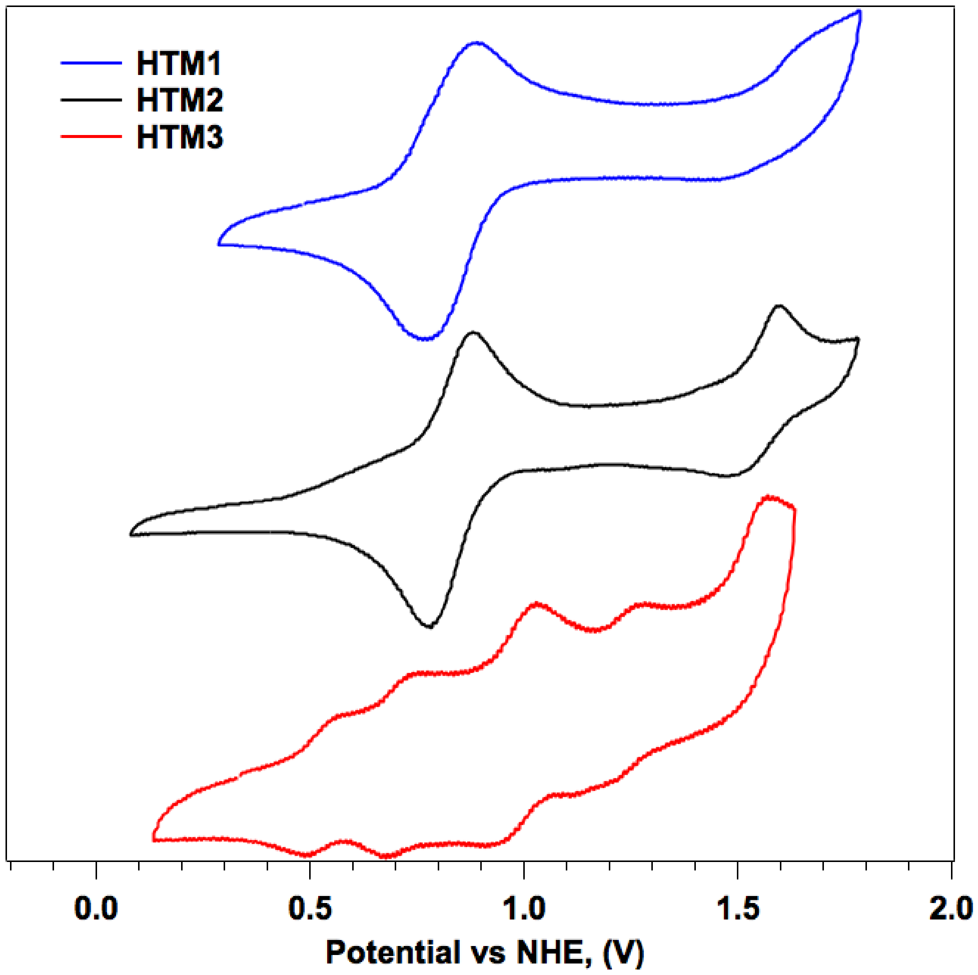

Figure S22. Cyclic voltammograms of the novel HTMs, **HTM1**, **HTM2** and **HTM3**.

Table S2. Electrochemical properties of **HTM1**, **HTM2** and **HTM3**.

Compound	$E_{1/2}^{ox1}$ [V][a]	E_{HOMO} [eV][b]
HTM1	0.88	–5.28
HTM2	0.89	–5.29
HTM3	0.57	–4.96

[a] Determined from CV measurements *vs.* normal hydrogen electrode (NHE). [b] E_{HOMO} was estimated in eV as E_{HOMO} = –4.44 eV – $E^{ox}_{1/2}$.

6. Differential Ideality Factor

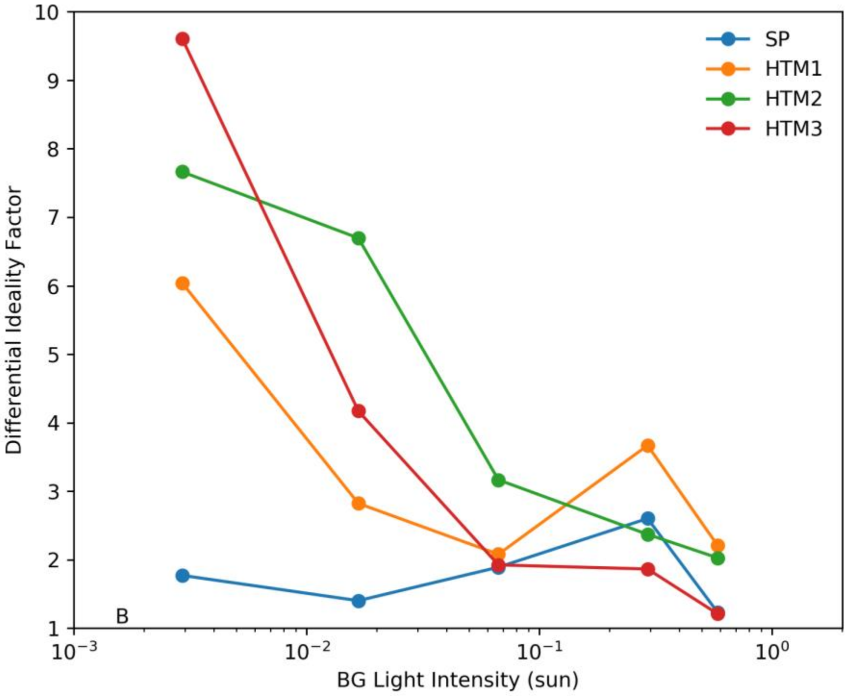

Figure S23. Differential Ideality Factor calculated by equation (4) in the main text.

7. TPC Fit

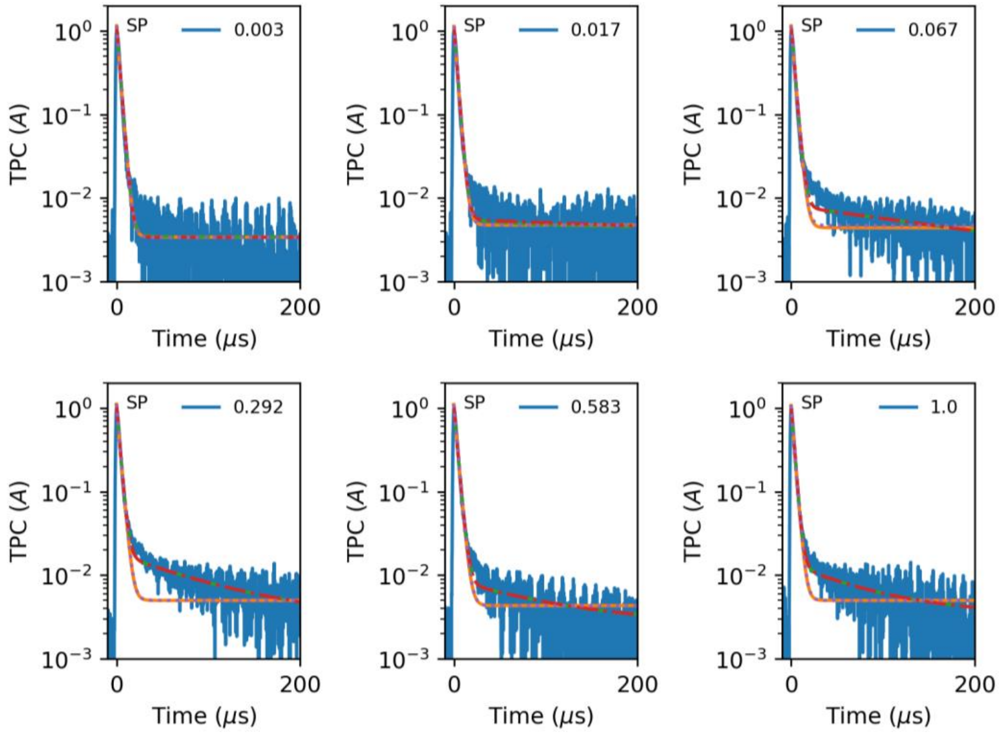

Figure S24. TPC fits of Spiro-OMeTAD (SP): Orange solid, green dash, red dash-dot and purple dot lines represent the fits by single, double, triple and stretched exponential decay functions, respectively. The legend indicates the BGL light intensity (sun).

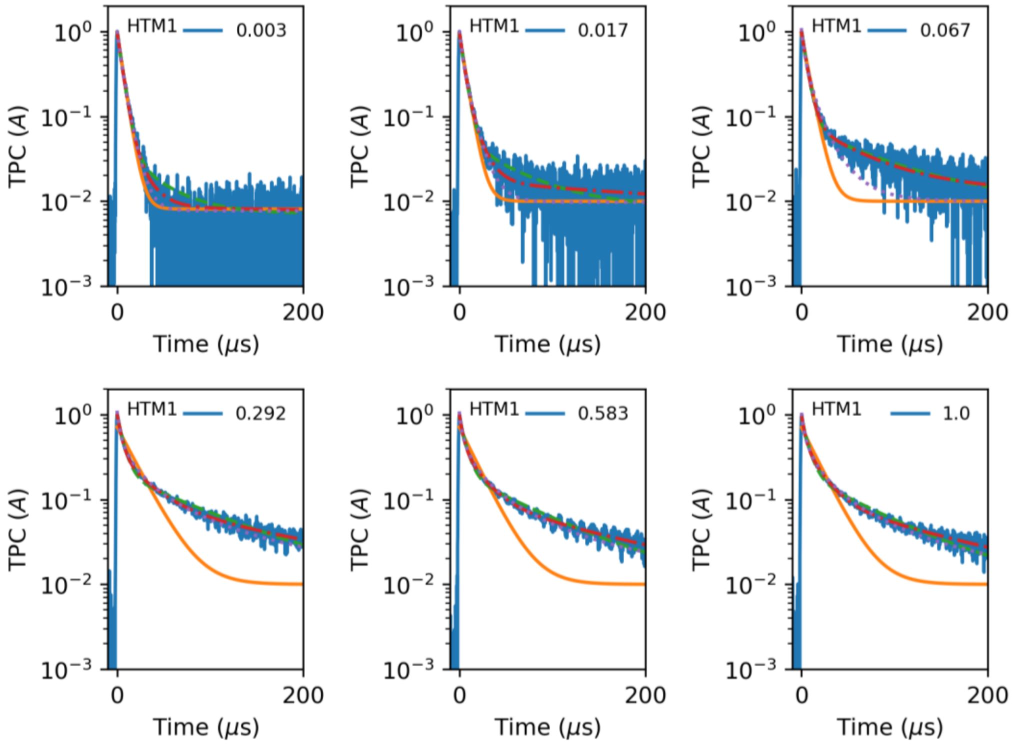

Figure S25. TPC fits of **HTM1**: Orange solid, green dash, red dash-dot and purple dot lines represent the fits by single, double, triple and stretched exponential decay functions, respectively. The legend indicates the BGL light intensity (sun).

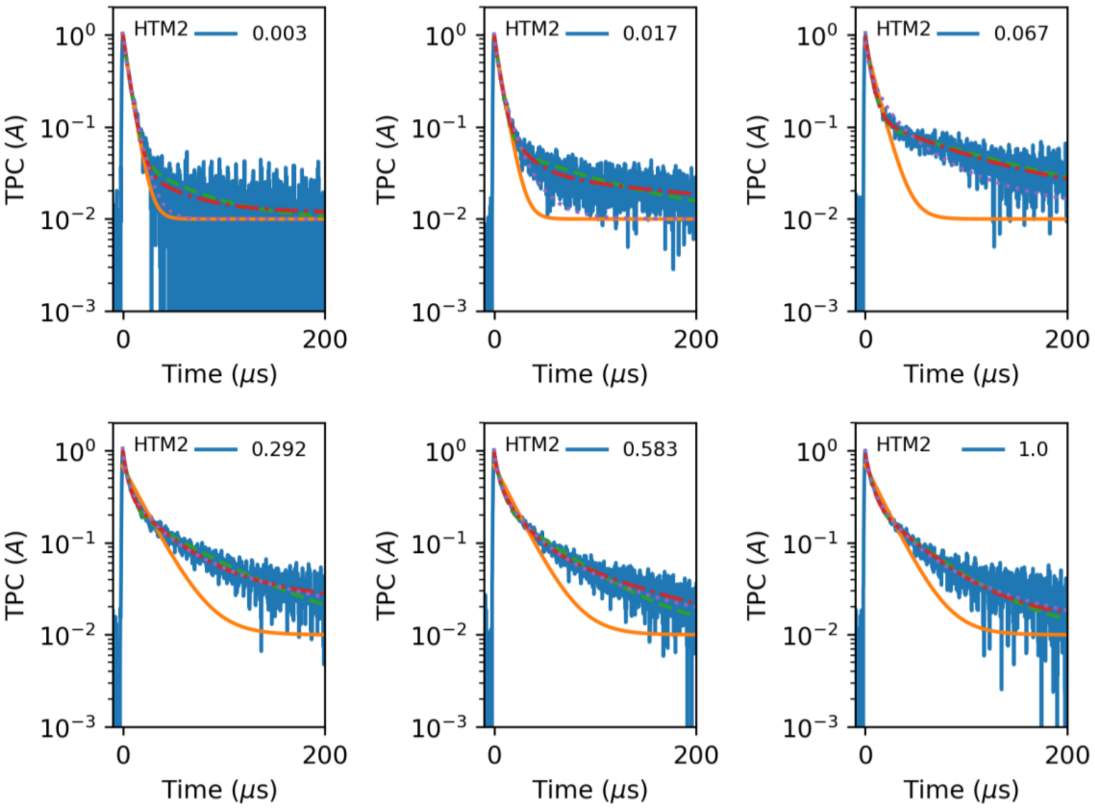

Figure S26. TPC fits of **HTM2**: Orange solid, green dash, red dash-dot and purple dot lines represent the fits by single, double, triple and stretched exponential decay functions, respectively. The legend indicates the BGL light intensity (sun).

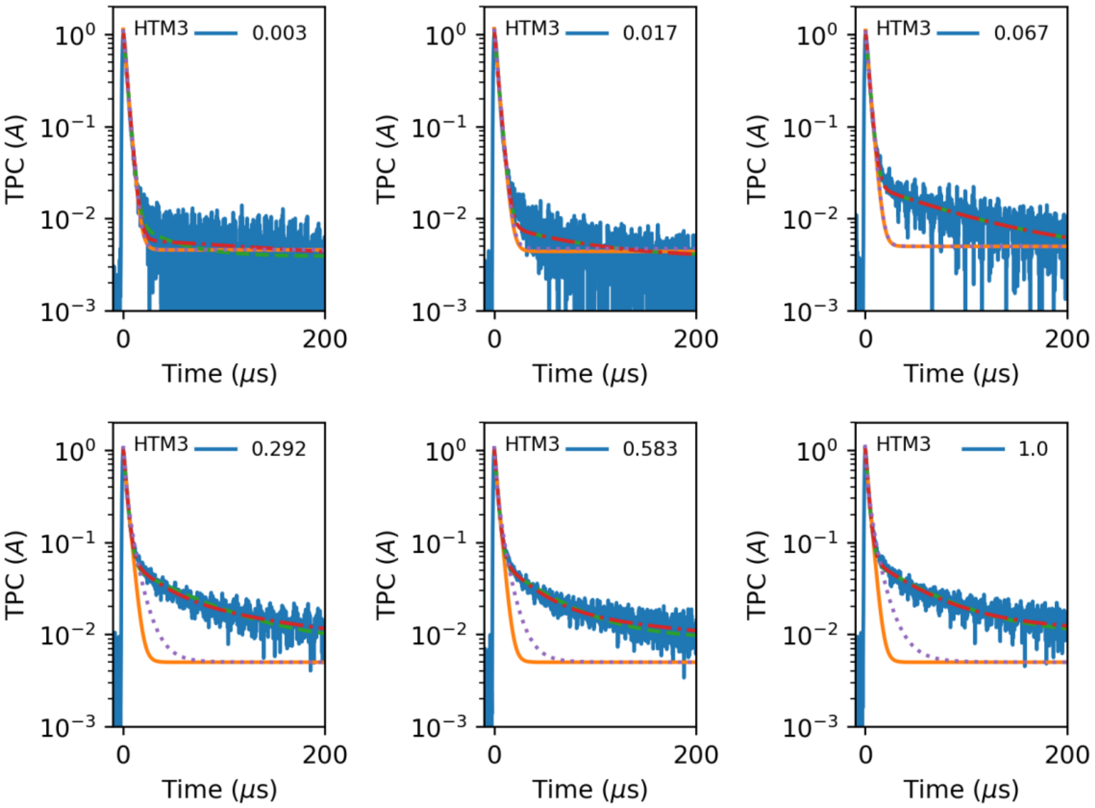

Figure S27. TPC fits of **HTM3**: Orange solid, green dash, red dash-dot and purple dot lines represent the fits by single, double, triple and stretched exponential decay functions, respectively. The legend indicates the BGL light intensity (sun).

8. TPV Fit

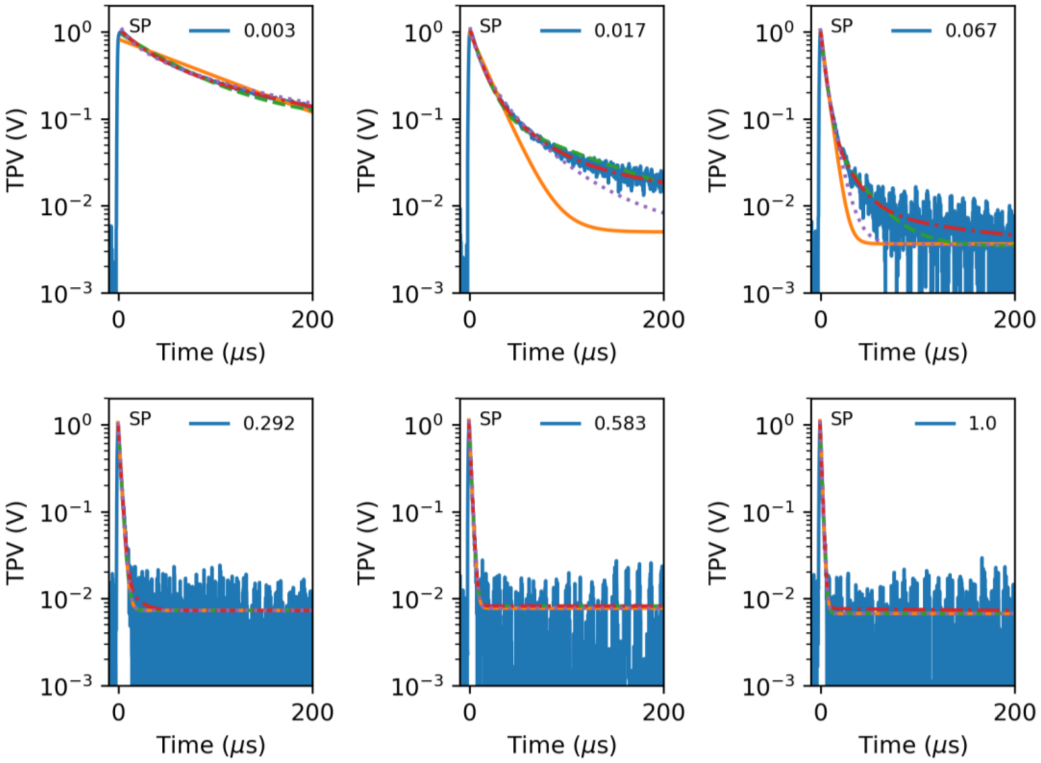

Figure S28. TPV fits of SP: Orange solid, green dash, red dash-dot and purple dot lines represent the fits by single, double, triple and stretched exponential decay functions, respectively. The legend indicates the BGL light intensity (sun).

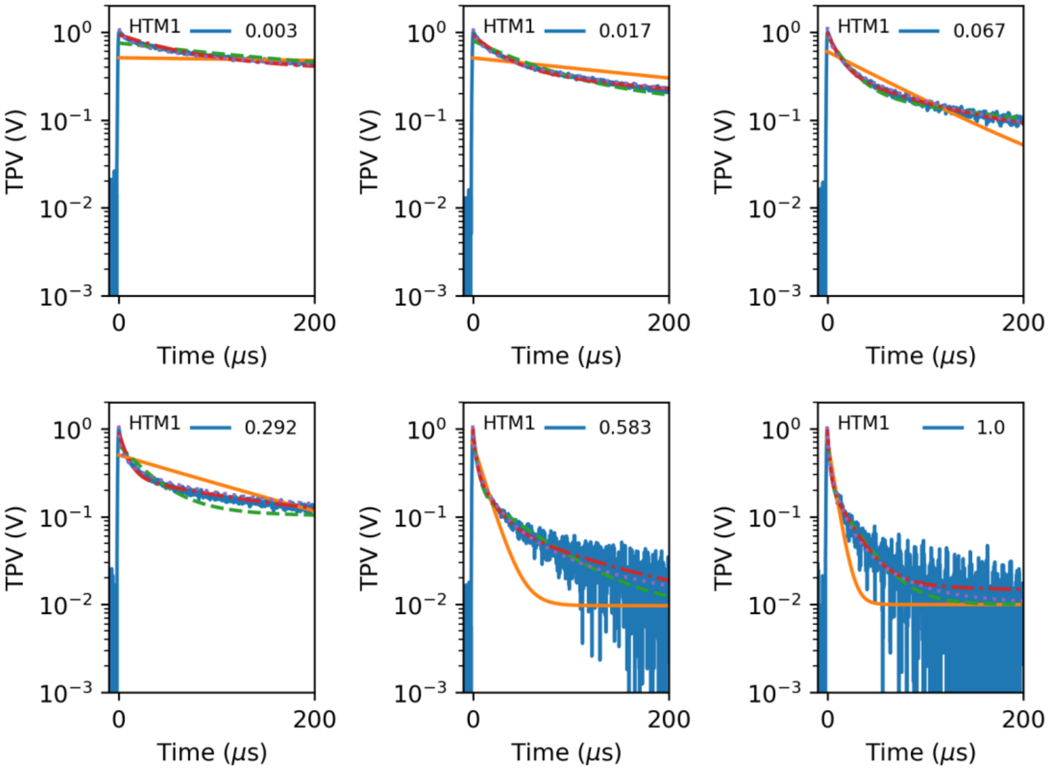

Figure S29. TPV fits of **HTM1**: Orange solid, green dash, red dash-dot and purple dot lines represent the fits by single, double, triple and stretched exponential decay functions, respectively. The legend indicates the BGL light intensity (sun).

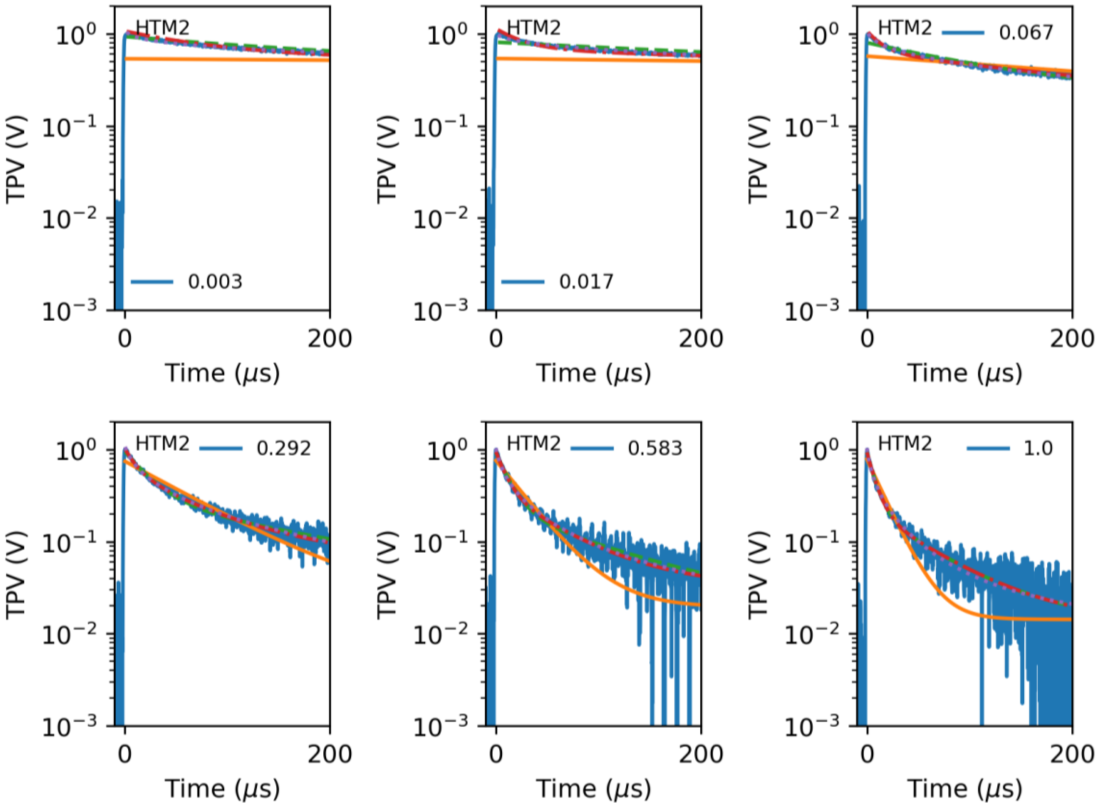

Figure S30. TPV fits of **HTM2**: Orange solid, green dash, red dash-dot and purple dot lines represent the fits by single, double, triple and stretched exponential decay functions, respectively. The legend indicates the BGL light intensity (sun).

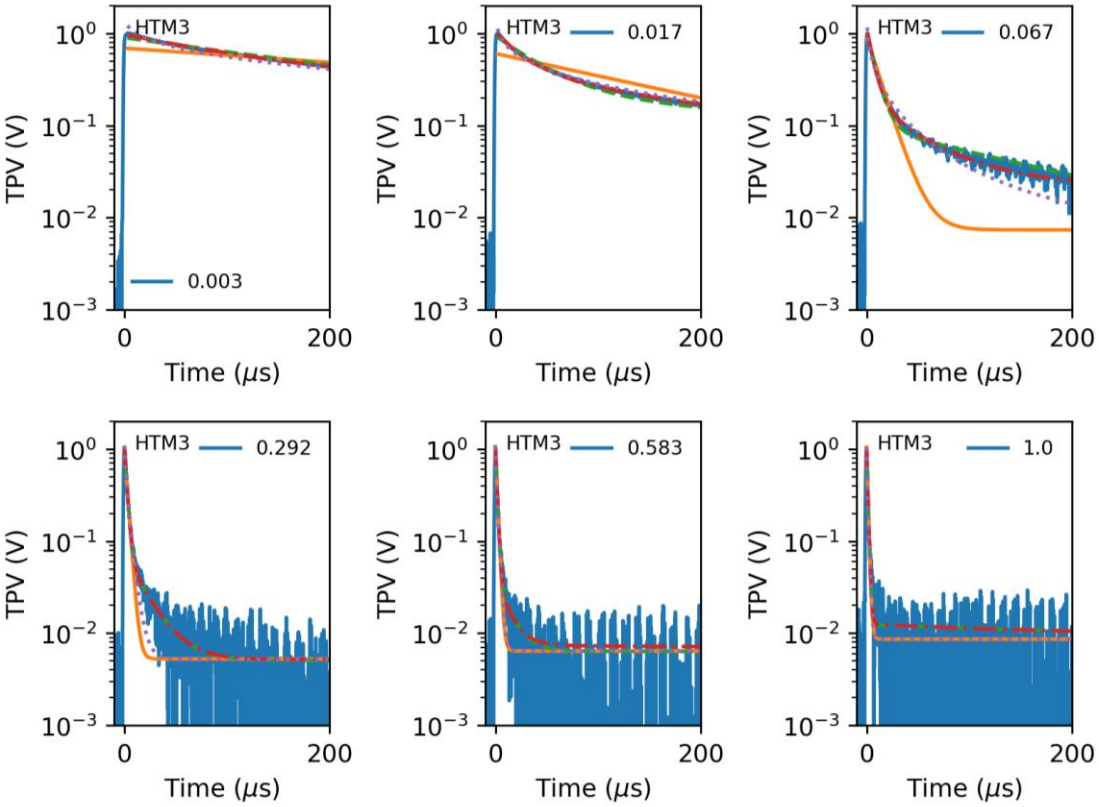

Figure S31. TPV fits of **HTM3**: Orange solid, green dash, red dash-dot and purple dot lines represent the fits by single, double, triple and stretched exponential decay functions, respectively. The legend indicates the BGL light intensity (sun).

9. TPC amplitudes as a function of BGL

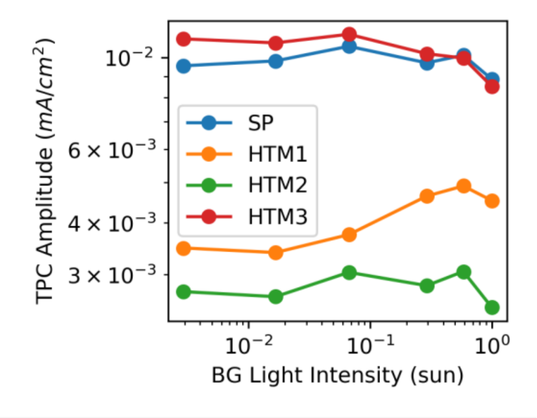

Figure S32. TPC amplitudes of the different HTMs as function of BGL.

10. Variation of Q (TPC integral) with BGL and integration time

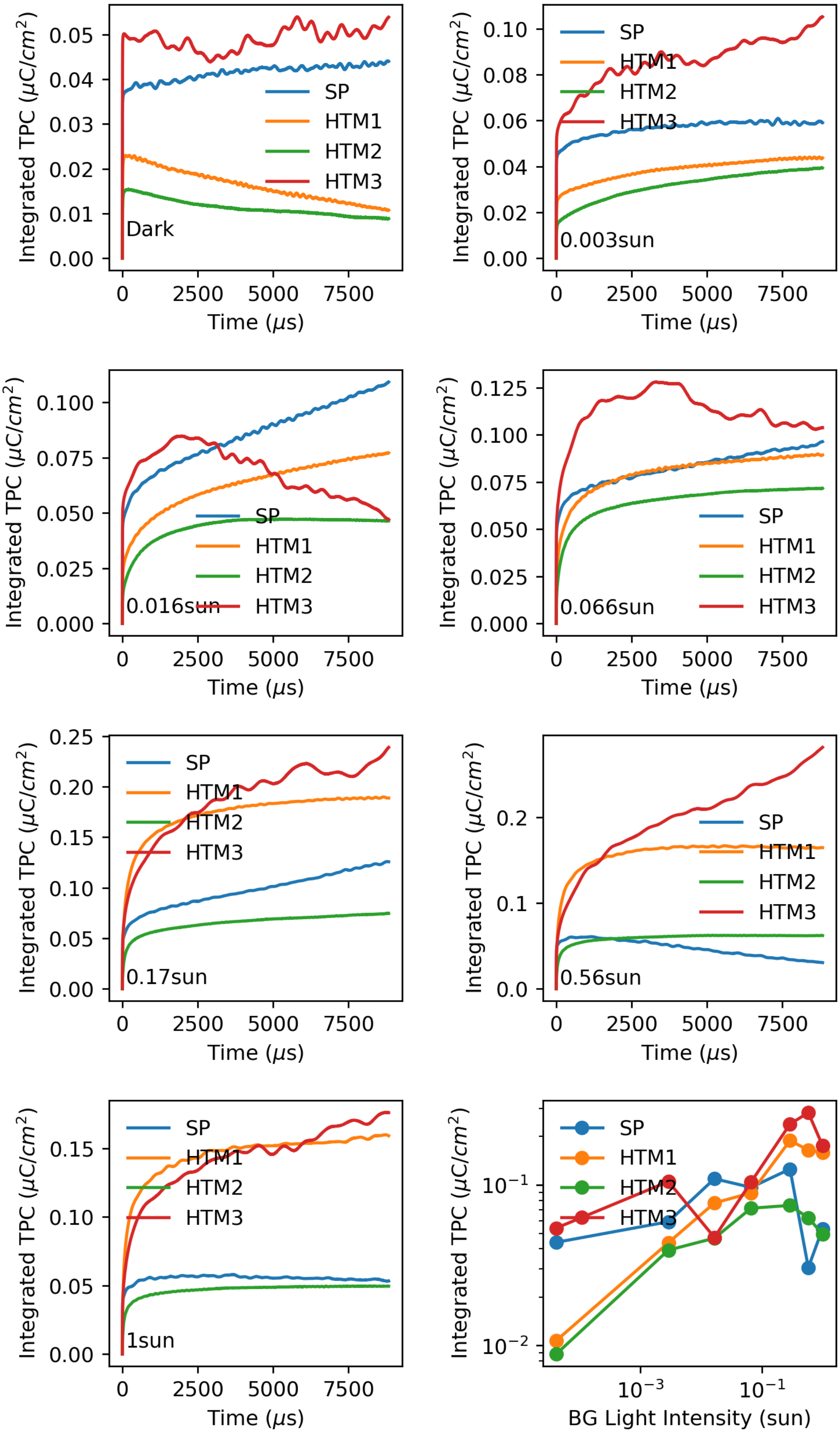

Figure S33. Integrated TPC (Q) *vs.* integration time for all HTMs.

11. I-V Curves / EQE

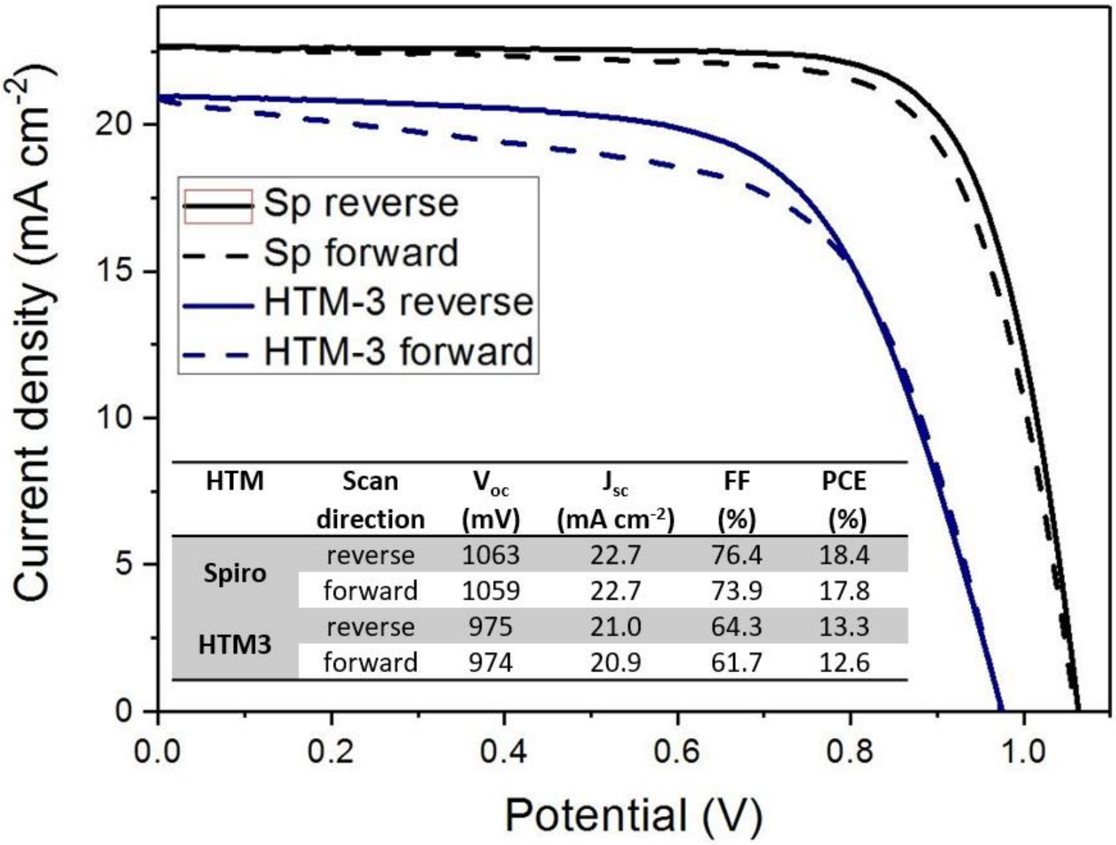

HTM	Scan direction	V_{oc} (mV)	J_{sc} (mA cm^{-2})	FF (%)	PCE (%)
Spiro	reverse	1063	22.7	76.4	18.4
	forward	1059	22.7	73.9	17.8
HTM3	reverse	975	21.0	64.3	13.3
	forward	974	20.9	61.7	12.6

Figure S34. I-V curves of the devices with Spiro-OMeTAD and HTM3 as HTM, and Cu as hole collection electrode instead of Au.

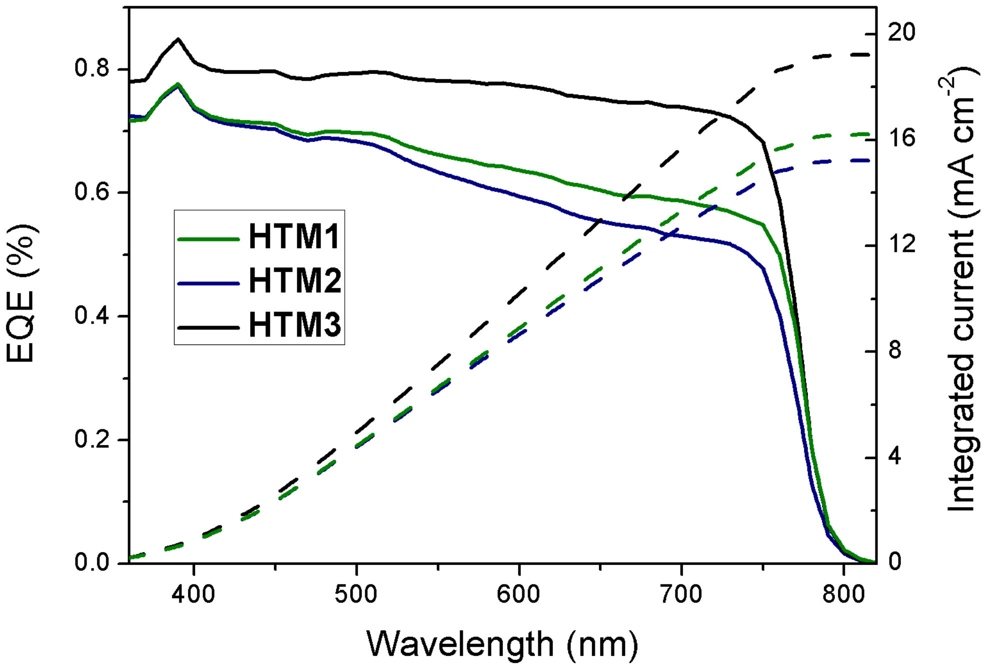

Figure S35. EQE data (solid lines) and integrated current densities (dashed lines) of the novel HTMs.

12. Simulation

12.1. Main Simulation Parameters

	ETM	Perovskite	HTM
Trap density ($m^{-3}\,eV^{-1}$)	5e22	5e22	5e22
Mobility ($m^{2}\,V^{-1}\,s^{-1}$)	1e-3	2e-3	1e-6
Relative permittivity	9	5	3
Density of states (m^{-3})	5e25	5e25	5e25
Bandgap (eV)	3.3	1.6	3.02
Free carrier recombination rate constant ($m^{3}\,s^{-1}$)	1e-16	1e-16	1e-16

12.2. Carrier Generation Rate

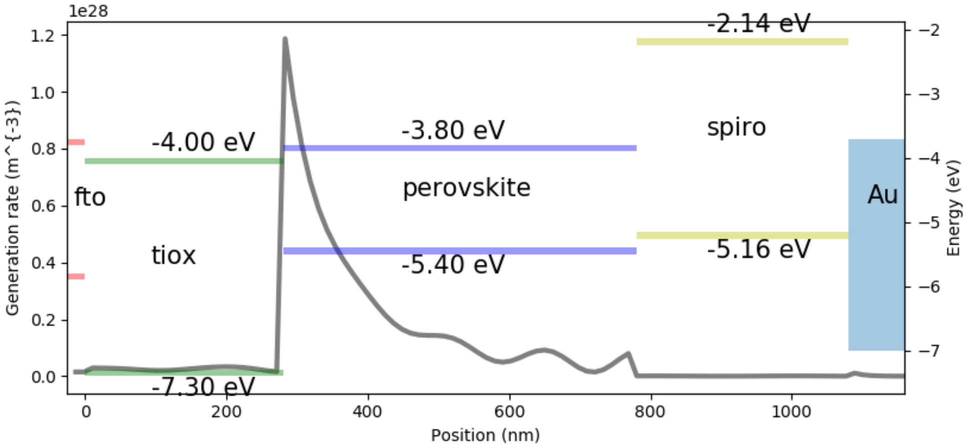

12.3. J-V curves for HTMs with different HOMO energy levels

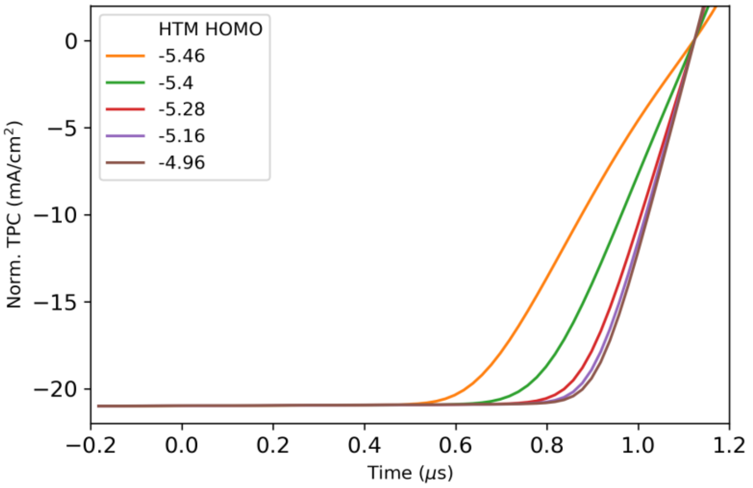

12.4. HTM trap-density/mobility/HOMO and device shunt resistance on ***V_{oc}***

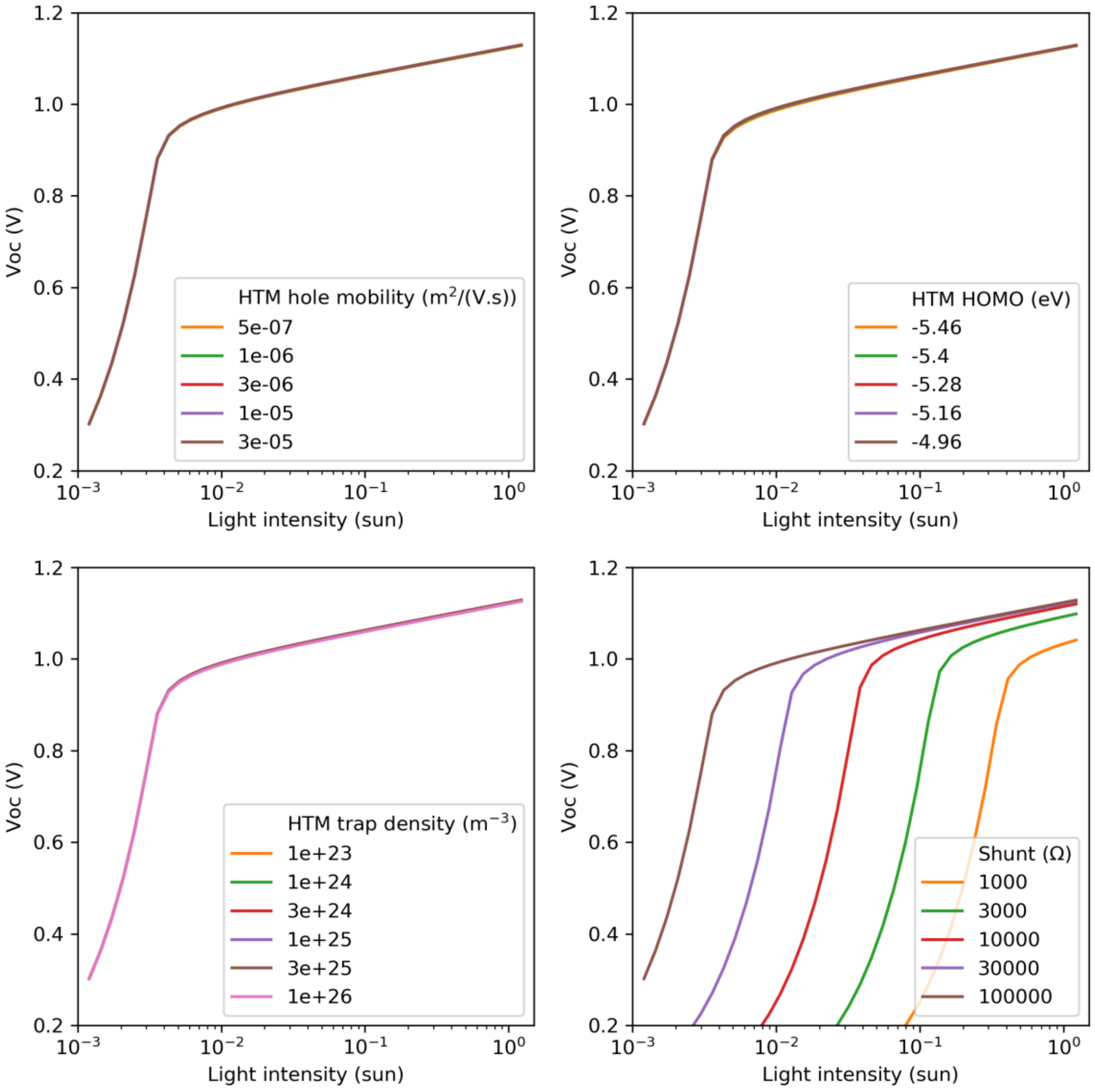

12.5. Impact of HTM trap-density/mobility/HOMO and series resistance on TPC at 0.1 sun

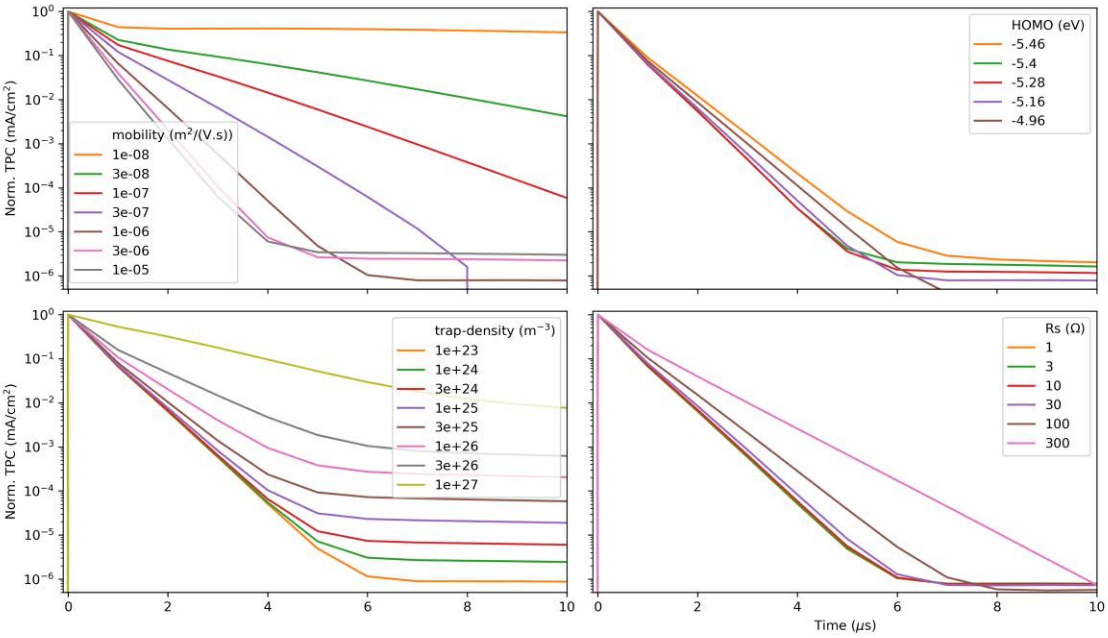

12.6. BGL intensity dependence of TPC under low/moderate/high HTM trap-density/mobility and series resistance

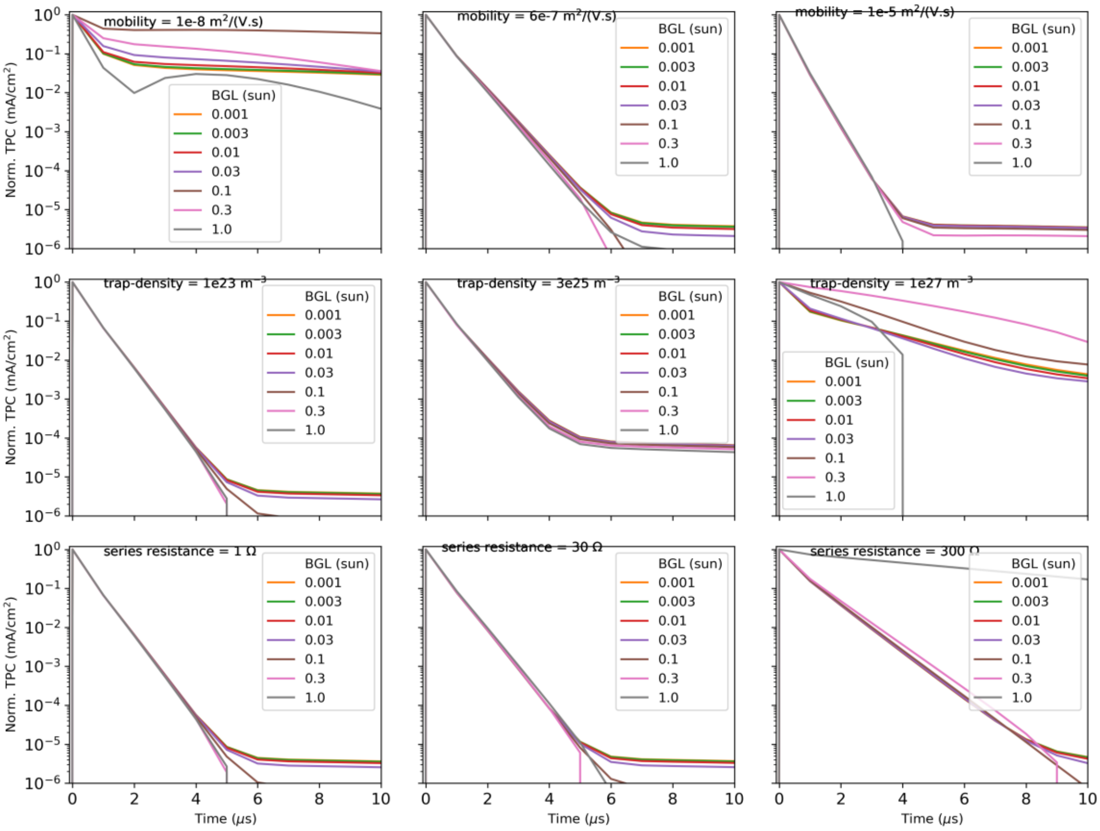

12.7. Impact of HTM trap-density/mobility/HOMO and shunt resistance on TPV at 0.1 sun

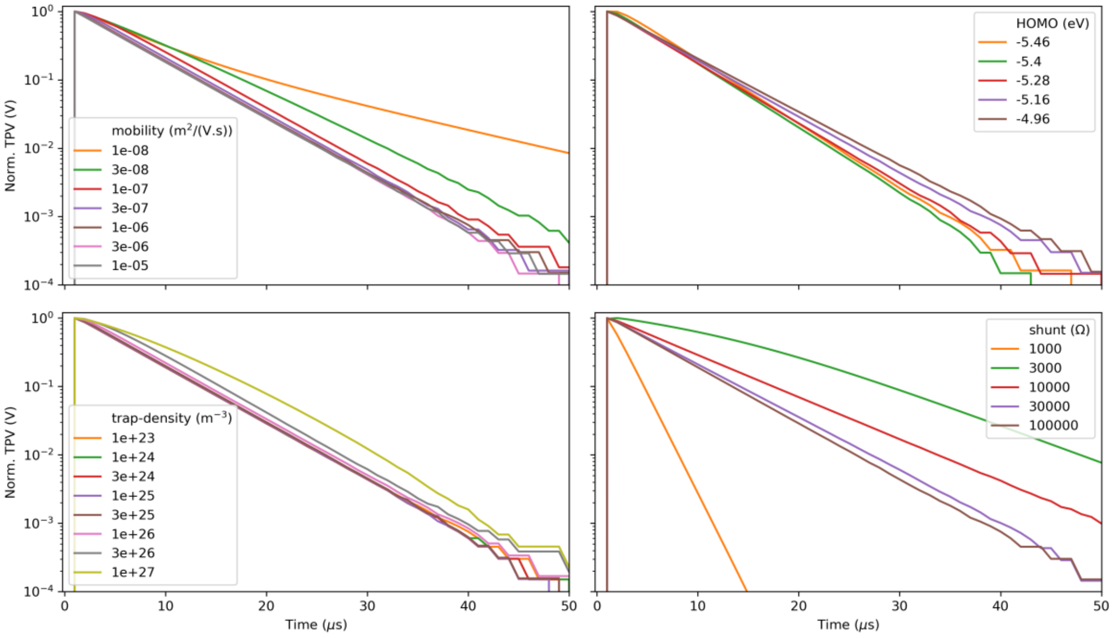

12.8. BGL intensity dependence of TPV under low/moderate/high HTM trap-density/mobility and shunt resistance

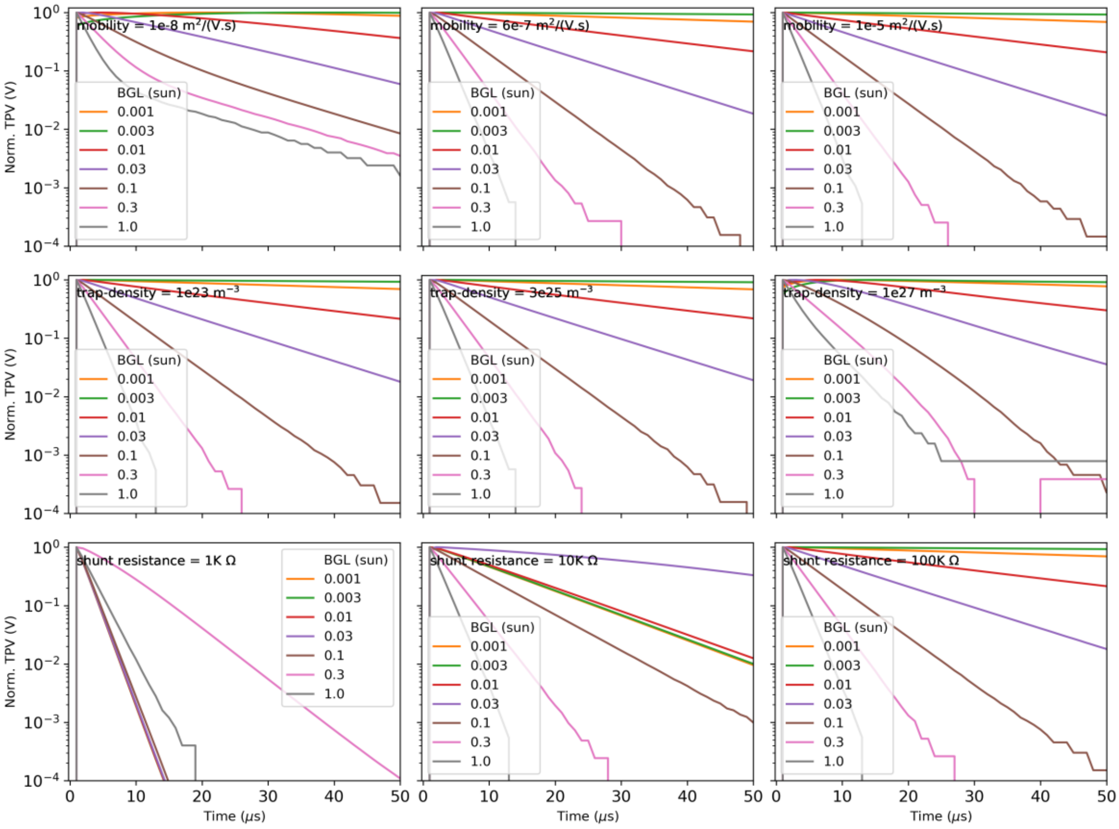

12.9. Impact of shunts on the BGL intensity dependence of TPV under moderate HTM trap-density